Electronic, structural, and optical properties of Y_2WO_6, a host material for inorganic phosphors

Pere Alemany [a] *and Jaime Llanos* [b]

Departament de Ciència dels Materials i Química Física and Institut de Química Teòrica i Computacional (IQTCUB), Universitat de Barcelona, Diagonal 647, 08028 Barcelona, Spain;

Departamento de Química, Universidad Católica del Norte, Avda. Angamos 0610, Casilla 1280, Antofagasta, Chile.

Tel: +34 93 403 1239; fax: +34 93 402 1231; e-mail: p.alemany@ub.edu (P.A.); Tel: +56 55 355624; fax: +56 55 355632; e-mail: jllanos@ucn.cl (J. L.)

[a] Universitat de Barcelona

[b] Universidad Católica del Norte

ABSTRACT

Optimization by first principles DFT-based electronic structure methods of the crystal structures for the five polymorphs of Y_2WO_6 reported in the literature yields results in good agreement with those determined experimentally by X-ray diffraction. The monoclinic *P*2/*c* phase appears to be the most stable one at ambient conditions, although high temperature orthorhombic phases with larger molar volumes could be favoured upon replacement of Y^{3+} cations by larger Ln^{3+} ones, and hence, provide plausible structures for Y_2WO_6:Ln^{3+} phosphors at ambient conditions. For all polymorphs the top of the valence band is dominated by O_{2p} orbitals with a relatively narrow WO_6-centred conduction band appearing just below a broad Y_{4d}-centred band. Insertion energies for Eu^{3+} replacing Y^{3+} are estimated to be in the range of 3 - 4 eV per cation, with the smaller values corresponding to substitutions into the larger octacoordinated Y^{3+} sites.

Keywords. Band structure, DFT calculations, Optical properties. Inorganic phosphor materials

1. Introduction

The fast development of new technological applications in the field of optoelectronics such as solid-state lighting devices (SSLD), plasma display panels, solar cells, or optical sensors has led to an intense research activity in the quest for new efficient luminescent materials in general, and rare-earth doped inorganic phosphors in particular. In the fabrication of white light emitting diodes (WLEDs), for instance, a fruitful approach has been to employ multiple layers of different rare-earth doped phosphors to down-convert the monochromatic UV or blue light generated by an electroluminescent diode into a broad-spectrum white light [1]. Recently there has been a notable interest in designing WLEDs by combining a near ultraviolet (n-UV) LED chip coupled with RGB phosphors (red, green, blue). In comparison with commercialized green and blue phosphors, red phosphors with lower reliability and poorer luminous efficiency have become the major challenge for n-UV light-emitting diodes. Some examples of recent research towards the fabrication of new red phosphors can be found in references [2-9]. The synthesis of new red phosphors has been shown to be also crucial in the development of novel LED devices to stimulate plant growth[10]. A very interesting application of inorganic phosphors that has received considerable attention recently is optical temperature sensing[11-13].

Inorganic rare-earth doped phosphors [14] consist typically in an inert host material, normally either an oxide such as $Y_3Al_5O_{12}$ (Yttrium aluminium garnet, YAG), nitrides/oxynitrides such as $Ba_3Si_6O_{12}N_2$, or sulphides/oxysulphides such as Y_2SO_2, which are doped with a small concentration of rare-earth ions that act as activators for the luminescence. Metal oxides containing d^0 transition metal ions, and in particular tungstates [15, 16], have received a considerable amount of attention in the last few years as host materials in the development of new phosphors, mainly due to their broad near-UV charge transfer bands and good thermal and chemical stabilities. When doped with trivalent Ln^{3+} lanthanide ions, rare-earth tungstate materials can be excited through the broad W–O charge transfer band, which is more efficient than exciting into the narrow parity-forbidden f–f transitions of the Ln^{3+} cations. Since the rare-earth tungstate matrix itself emits in the blue-green region [17] one of the promising applications of tungstate based phosphors is the possibility to obtain white light emission from a single material by a adequate combination of the narrow-line emission of the doped Ln^{3+} ions with the broad-band emission of the matrix.

Among tungstate materials used in the development of new phosphors, Y_2WO_6 has received a considerable attention recently. Yttrium tungstate has been proposed as a suitable matrix for red phosphors [18-21], or for the fabrication of white light-emitting diodes [22-27]. The up conversion process in Y_2WO_6 based phosphors [28-31] has also received some attention, with suggestions for application in solar cells [32] or optical thermometry[33-35]. Y_2WO_6 has also been found to be a suitable matrix for the fabrication of phosphors with a controlled structure at the nanoscale [36-41].

In the past few years, we have been actively involved in the preparation of new phosphors, and in particular, $Y_{2-x}Eu_xWO_6$ red phosphors [42, 43]. $Y_{1.86}Eu_{0.14}WO_6$, for example, has been successfully applied to increase the spectral response of dye-sensitized solar cells by incorporating it as a down-conversion material into TiO_2 photoelectrodes [44].

The local chemical environment of the dopant activator ions is one of the key factors determining the optical properties of inorganic phosphors. Since in most cases it is almost impossible to obtain detailed information on this local environment in the actual phosphors, we have found that combining the experimental work with accurate DFT-based first principles calculations may yield interesting complementary information for the design and characterization of new phosphors. Following our previous work on various Y and La oxides and oxysulphides [45] we present here a computational study of the electronic structure of the five polymorphs of Y_2WO_6 that have been described in the literature, complemented with a detailed description of the principal crystallochemical parameters of the different sites for Y in each structure and an evaluation of the effects of Y replacement by Eu in order to gain some information about the most plausible coordination environments of Eu^{3+} cations in these phosphors.

2. Computational details

Electronic structure calculations were carried out using a numerical atomic orbitals approach based on density functional theory (DFT) which has been developed and designed for efficient calculations in large systems and implemented in the SIESTA code [46-48]. We have used both the local density approximation (LDA) [49, 50] as well as the generalized gradient approximation (GGA) to DFT and, in particular, the PBE[51] and PBEsol [52] functionals. In calculations including Eu atoms, a Hubbard correction [53, 54] term, $U_{eff} = 7$ eV, has been introduced for the 4f orbitals on these atoms and spin polarization has been taken into account forcing a total of six unpaired spins on each Eu^{3+} ion.

Only the valence electrons are considered in the calculation, with the cores being replaced by norm-conserving, scalar relativistic pseudopotentials [55] factorized in the Kleinman-Bylander form [56]. We have used an energy shift of 50 meV[57] to generate split-valence double-ζ basis sets including polarization orbitals for Y, Eu, and O atoms, and split-valence triple-ζ basis sets with polarization functions for W and Bi ones. The semicore 4s, 4p, and 4d electrons in Y were also treated explicitly and the corresponding orbitals described by single-ζ basis functions.

The energy cutoff of the real space integration mesh was set to 250 Ry in all calculations. The SCF procedure was considered to converge when the difference in the density matrix elements between two successive cycles was below 10^{-4}. For all structures with Z=4 (36 atoms in the unit cell), the Brillouin zone was sampled using a grid of 296 *k*-points generated with the Monkhorst-Pack algorithm[58]by a diagonal (8×8×8) matrix. For the orthorhombic phase with Z=8 a reduced set of 150 *k*-points, generated by a (8×4×8) matrix, was used. Structural optimizations were performed using the conjugate gradients method with a maximum displacement of 0.1Å and a tolerance factor for the maximum force of 0.04 $eVÅ^{-1}$. The imaginary part of the dielectric function, $\varepsilon_2(\omega)$, has been obtained by the simplest approach based on the calculation of the dipolar transition matrix elements between different eigenfunctions of the self-consistent Hamiltonian, carried out in the momentum space formulation. The real part of the dielectric function, $\varepsilon_1(\omega)$, is extracted from $\varepsilon_2(\omega)$ using the Kramers-Kronig relation. Calculation of optical properties has been performed for polycrystalline sample with a broadening factor of 0.1 eV to simulate experimental conditions.

The geometry of the coordination environment of the Eu^{3+} ions is crucial for the fine-tuning of the optical properties of the doped materials and we will describe it using continuous shape and symmetry measures (CShM and CSM, respectively)[59, 60]. These measures describe in a quantitative way the degree of distortion of the coordination sphere around a given atom with respect to the shape of a predefined ideal polyhedron or symmetry, respectively. To obtain the CShM for a given N-vertex polyhedron *Q* with respect to an ideal polyhedron *P* with the same number of vertices, the two polyhedra are superimposed in such a way that the sum of squared distances between their vertices is minimized. The expression for the CShM of *Q* with respect to the ideal polyhedron *P* is given by [60, 61]

$$S(Q,P) = min\frac{\sum_{i=1}^{N}|\boldsymbol{q}_k-\boldsymbol{p}_k|^2}{\sum_{i=1}^{N}|\boldsymbol{q}_k-\boldsymbol{q}_0|^2}\cdot 100 \qquad (1)$$

where $\mathbf{q}_k$ and $\mathbf{p}_k$ are the coordinates for the vertices of *Q* and *P*, respectively, and $\mathbf{q}_0$ the geometric centre of *Q*. The actual value of $S_P(Q)$ is found by searching for the translation, rotation, relative size, and vertex pairing that minimize the sum of squared distances between the vertices of *P* and *Q*. From equation [1] it follows that if *Q* has exactly the same shape as *P*, then $S_P(Q) = 0$. Since $S_P(Q)$ is always positive, the larger the value of $S_P(Q)$ the less similar is *Q* to the ideal shape *P*. It can be shown that the maximum value that $S_P(Q)$ can attain is 100, corresponding to the case where all vertices of *Q* collapse into a single point[61].

The continuous symmetry measure $S_G(Q)$ for a polyhedron *Q* relative to a given symmetry point group *G* is defined in a similar way to the shape measure[62, 63], comparing now the problem structure *Q* with its transformed images resulting from applying all the symmetry operations of symmetry group *G* on *Q*. The definition of $S_G(Q)$ is analogous to that of $S_P(Q)$ in equation [1] replacing the coordinates $\mathbf{p}_k$ of the reference polyhedron by those of the closest structure to *Q* with the desired *G*-symmetry. In this case, the minimization process included in the definition of the measure refers to the orientation of the symmetry elements generating the symmetry operations in *G*, as well as the pairing of the vertices of *Q* with those of its transformed image. Note that in contrast to the CShM, where the reference structure *P* is known previously, in the case of the CSM, the reference *G*-symmetric structure must be determined in the process of calculating $S_G(Q)$. As in the case of the shape measures, an $S_G(Q)$ value of 0 indicates that *Q* is *G*-symmetric, while the larger the value of $S_G(Q)$, the larger is the departure of *Q* from having *G*-symmetry. In the following, since there is no confusion about the structure *Q* for which the CShMs and CSMs are calculated, to avoid using complicated subscripts we will simply use *S(P)* and *S(G)* for $S_P(Q)$ and $S_G(Q)$, respectively. For instance, for a given polyhedron, *S(OC)* will be the corresponding octahedral CShM and $S(C_i)$ the CSM used to check the departure from centrosymmetry.

The main purpose of using CShMs and CSMs is to characterize the shape and symmetry of complex coordination geometries with just a few parameters [64-68] and for this we take a reference shape, for instance an octahedron, and calculate the octahedral shape measure *S(OC)* for the experimentally found distorted structures. Although CShM and CSM values can fall in the range between 0 and 100, the measures for severely distorted chemical structures are never larger than 50. As a rule of thumb we can say that chemically significant distortions lead to shape or symmetry measures about 0.1 or higher, while values larger than 3 indicate important distortions. In our case a very important measure is the departure from a centrosymmetric coordination environment as measured by $S(C_i)$ since this will allow mixing of formally '*g*' and '*u*' functions that will influence greatly the optical properties of the material. Since independently of the reference shape and the number of vertices all CShM and CSM values are on the same scale, we can compare, for instance the deviation of a given structure from different reference shapes, or of different structures with respect to the same ideal shape or symmetry to decide which is the best description for the shape and symmetry in each case.

3. Results and discussion

3.1 Crystal structures

To the best of our knowledge, five alternative crystal structures have been reported for Y_2WO_6:Ln^{3+} phosphors. They belong to four different space groups, namely, one monoclinic *P2/c* (n. 13) phase, two orthorhombic $P2_12_12_1$ (n. 19) polymorphs with different unit cells (Z=4 and Z=8, respectively), an orthorhombic $P2_1ab$ (n. 29) phase, and a tetragonal *P4/nmm* (n. 129) one [15, 42, 69, 70]. Using the experimental crystal structures (the related Bi_2WO_6 structure was used for the orthorhombic $P2_1ab$ polymorph) as an initial guess, we have performed a complete structural optimization allowing simultaneous changes both in the cell parameters and the internal coordinates for a single unit cell (Z=4 with 36 atoms for all cases except for the orthorhombic $P2_12_12_1$ polymorph, with Z=8 and 72 atoms in the unit cell) without imposing any symmetry restrictions. The crystal structures were optimized considering three different density functionals for the calculation of the electronic structure: the local LDA functional and the two GGA-type functionals, PBE and PBEsol. The structure of the local coordination environments of the W and Y atoms has been also analysed using the average M-O distances (M = W, Y, Eu) to estimate their average size and the CShMs with respect to different polyhedra: the octahedron (O_h symmetry) and the trigonal prism (D_{3h} symmetry) for coordination number 6, the capped octahedron (C_{3v} symmetry) and a trigonal prism capped on one of the square faces (C_{2v} symmetry) for coordination number 7, and the cube (O_h symmetry), the square antiprism (D_{4d} symmetry), and the triangular dodecahedron (D_{2d} symmetry) for coordination number 8. Since most of our interest is in the local symmetry of the coordination sites for Eu^{3+} ions in the phosphors obtained from Y_2WO_6, we have also computed the inversion symmetry measure $S(C_i)$ for each site, considering for this purpose the central metal atom and the polyhedron made from the nearest O atoms.

In all optimizations the symmetry of the initial guess structure is preserved up to numerical error and, hence, the coordination environments of symmetry equivalent atoms remain the same. As expected for highly isotropic, fairly ionic structures such as in this case, for each polymorph we find in our optimizations similar deviations from experimental values for the three *a, b*, and *c* cell parameters, regardless of the functional employed (see tables S1 to S5 in the supplementary material for the actual values obtained in all the optimizations. As a general trend we observe the well-known behaviour of the LDA functional to yield too small unit cells, while the GGA functionals tend to overestimate their size. In order to minimize differences between the polymorphs due to experimental or computational errors, as a compromise, we will use the optimal structures obtained with the PBEsol functional, slightly larger than the experimental ones, for all further calculations. Very similar results were obtained using either the experimental structures or those obtained in optimizations with the other two functionals. Before discussing these results we will present a more detailed discussion of the principal structural features for each of the studied polymorphs.

Monoclinic *P2/c* polymorph. In most studies reported up to date, both pure Y_2WO_6 and $Y_2WO_6{:}Ln^{3+}$ crystals are found to adopt the *P2/c* (n. 13) monoclinic (**m-13**) polymorph [71-73]. As it may be appreciated in Fig. 1a, Y^{3+} occupies three non-equivalent sites, two of them with eight O^{2-} ions in the first coordination sphere (Fig.s 1b and 1c), and the other one coordinated by seven O^{2-} ions (Fig. 1d). Each of the symmetry equivalent W^{6+} ions in the unit cell is surrounded by six oxygen atoms forming a distorted WO_6 octahedron (Fig. 1e).

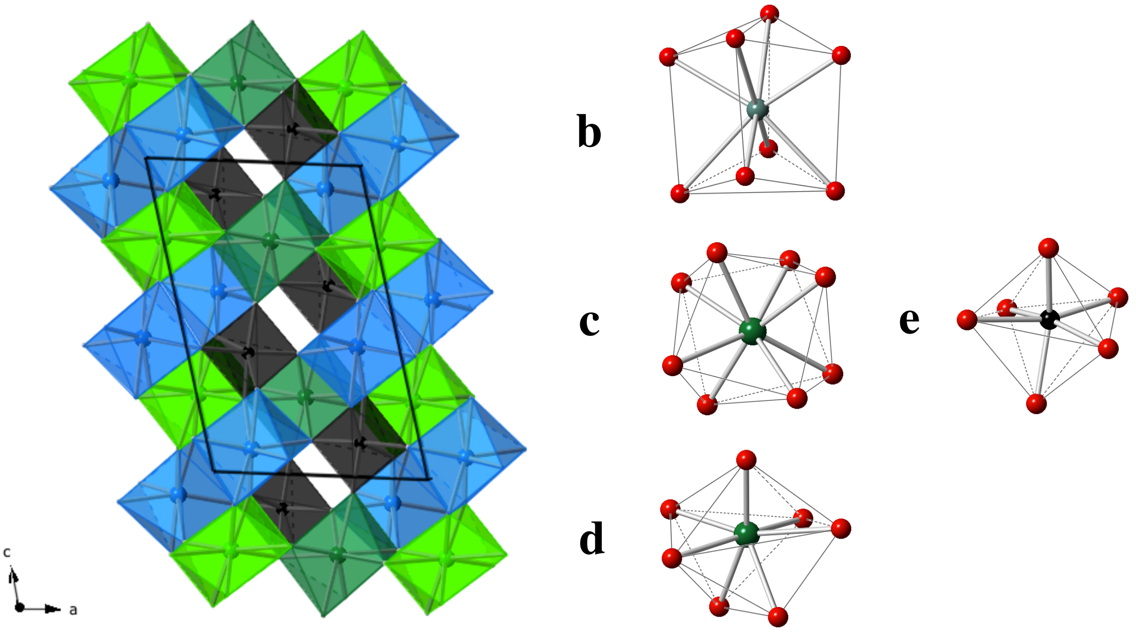

Fig. 1 Monoclinic **m-13** crystal structure for Y_2WO_6 [71]. a) View of the complete structure along the crystallographic *b* axis highlighting the different coordination polyhedra: eight-coordinated Y atoms in bright and dark green, seven-coordinated Y atoms in blue and W atoms in black. b) Coordination environment for Y atoms in the Y1 sites, c) in the Y2 sites, d) in the Y3 sites, and e) for W atoms.

The unit cell parameters obtained in the optimization for the **m-13** polymorph are given in the supplementary material (table S1) together with the experimentally determined values. Agreement between the optimized structure and the experimental one is highly satisfactory, especially for the LDA functional. Although optimization with the PBEsol functional yields a slightly overestimated volume for the unit cell, the error, 1.4%, is small if compared with those obtained for similar compounds and the PBEsol structure can be safely used to study the electronic structure for all studied polymorphs of Y_2WO_6, while the LDA functional, although giving the best agreement with the experimental structure for the particular case of the **m-13** phase, leads to larger underestimations of the volume for the other polymorphs (see tables S1 to S5 in the supplementary material).

Information about the shape and symmetry of the coordination sphere for the W and Y atoms in the **m-13** polymorph is given in table 1. The experimental size (estimated by the average M-O distance) and shape of the coordination environments of all metal atoms is quite well reproduced in the PBEsol optimized structure.

site		d_{M-O} (Å)	S(OC)	S(TP)	S(COC)	S(CTP)	S(CU)	S(SAP)	S(TDD)	S(C_i)
W	exp.	1.940	4.314	5.109	-	-	-	-	-	3.788
	calc	1.968	4.567	4.954						3.970
Y1 (2e)	exp.	2.355	-	-	-	-	2.906	4.272	2.899	2.215
	calc.	2.355					2.674	4.370	2.716	2.140
Y2 (2f)	exp.	2.373	-	-	-	-	5.002	1.717	1.954	4.939
	calc	2.375					4.926	1.680	1.806	4.871
Y3 (4g)	exp.	2.305	-	-	1.852	1.695	-	-	-	15.947
	calc.	2.305			1.822	1.667				15.992

Table 1 Experimental [71] and optimized (PBEsol functional) structures for the coordination environments of Y^{3+} and W^{6+} in the **m-13** polymorph of Y_2WO_6. The d_{M-O} values in the third column refer to average M-O (M = W or Y) distances for each polyhedron. Labels for reference

polyhedra in the shape analysis are: for coordination number 6, OC for the octahedron and TPR for the trigonal prism; for coordination number 7, COC for the capped octahedron and CTP for the capped trigonal prism; and for coordination number 8, CU for the cube, SAR for the square antiprism, and TDD for the triangular dodecahedron. The $S(C_i)$ value in the last column corresponds to the departure from inversion symmetry as measured by the corresponding CSM.

Analysis of the distribution of W-O distances shows that the W atoms (Fig. 1e) occupy six coordinated sites. Although the smallest shape measure is that for the octahedron, the large value of this measure, about 4.5, points to a strong distortion from the ideal octahedral geometry that is also reflected in the value of $S(C_i) \approx 4.0$, which should be exactly 0.0 for a perfect octahedron. Since S(TP) is not much larger than S(OC), the best description for the shape of the coordination environment of W is that of an intermediate structure between that of an octahedron and a trigonal prism. A quantitative analysis of the CShM values shows indeed that the coordination polyhedron for the W^{6+} ions lies approximately halfway in the minimal distortion path [61] between these two polyhedra, with a generalized interconversion coordinate around 50.0 and a deviation from the minimal distortion path of about 4%.

In the **m-13** polymorph, two of the distinct Y ions are octacoordinated, while in the other one it is heptacordinated. The average Y-O distances are very close in the three cases, but, as expected, slightly larger in the eight coordinated sites. The shape analysis indicates that the coordination geometry of the Y1 site can be described either as that of a distorted cube or as that of a distorted triangular dodecahedron, since both shape measures are quite similar. In this case the geometry does not lie on the minimal distortion path between these two ideal polyhedra. The inversion measure, around 2.0, is closer to that of an ideal cube (0.0) than to that of the reference triangular dodecahedron (7.9) so that the best description for the coordination polyhedron at the Y1 sites is that of a distorted cube.

The coordination polyhedron at the Y2 sites (Fig. 1c) has an intermediate geometry between that of a cube and a square antiprism, lying approximately halfway in the minimal distortion path [61] between these two polyhedra. The generalized interconversion coordinate (≈ 66%) shows that the structure is closer to the antiprism than to the cube. The $S(C_i)$ value around 5.0 for this site is also in between that of a cube (0.0) and that for the reference square antiprism (10.8) and somewhat larger than that corresponding to the other octacordinated Y1 sites.

Atoms in the Y3 sites are heptacordinated, with the smallest shape measure for the capped triangular prism, although a quite similar value is found for the capped octahedron. Further analysis indicates that in this case the structure is not on the interconversion path between the two polyhedra and the simplest description for it is that of a distorted capped triangular prism. The $S(C_i)$ value around 15.0 indicates a strong departure from a centrosymmetric environment as expected for a coordination polyhedron with an odd number of vertices, although the calculated value is significantly smaller than those obtained for the reference capped octahedron (20.2) or capped triangular prism (20.3).

Orthorhombic $P2_12_12_1$ (Z = 4) polymorph. Three different orthorhombic polymorphs have been described for either Y_2WO_6 or $Y_2WO_6:Ln^{3+}$ crystals. Two of them adopt the $P2_12_12_1$ (n. 19) spacegroup. The first of them (**o-19-z4**) was described by Tyulin et al. [74] and contains four formula units in the unit cell (Z=4) with Y occupying two different types of heptacordinate sites (Fig. 2). Optimization with all three functionals leads to quite similar structures, with a somewhat smaller unit cell for the LDA functional and the two GGA functionals overestimating its volume slightly (Table S2 in the supplementary material). The errors in the three cell parameters are also of the same magnitude in all optimizations, indicating that cohesive forces are very isotropic, as expected for a compact highly ionic structure such as this.

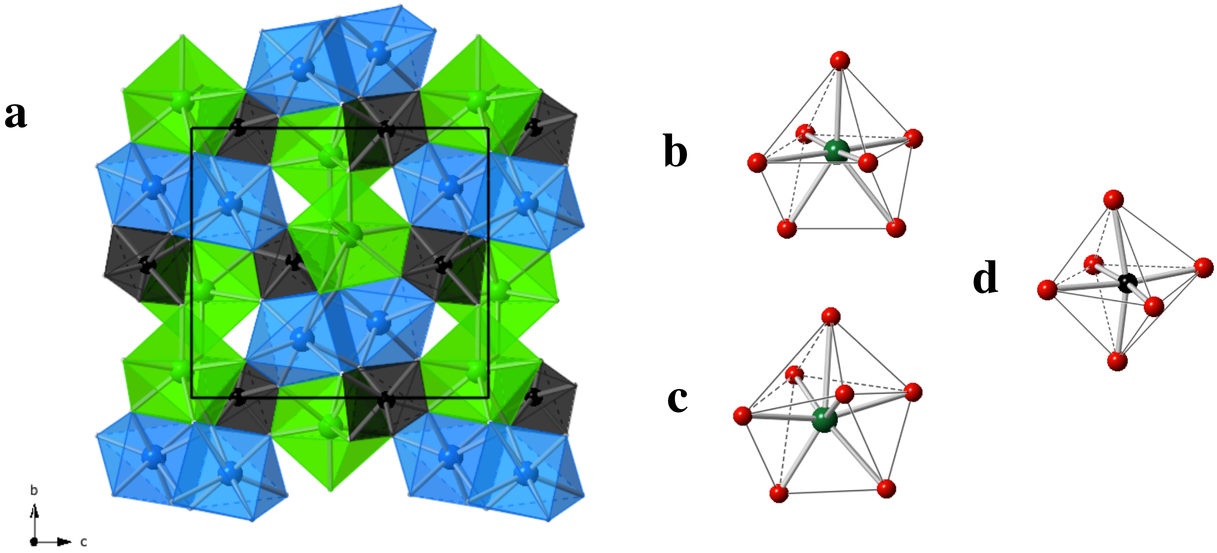

Fig. 2 Orthorhombic **o-19-z4** crystal structure for Y_2WO_6 [74]. a) View of the complete structure along the crystallographic *a* axis highlighting the different coordination polyhedra:

eight-coordinated Y atoms in bright green, seven-coordinated Y atoms in blue and W atoms in black. b) Coordination environment for Y atoms in the Y1 sites, c) in the Y2 sites, and d) for W atoms.

The analysis of the distribution of the W-O distances shows that the W atoms (Fig. 2d) occupy six coordinated sites with a fairly regular octahedral geometry as it can bee deduced from the shape measures in table 2. Deviation from ideal octahedral symmetry is due to a distortion towards the trigonal prism (Bailar distortion)[75] with a generalized interconversion coordinate around 25%, much closer to the octahedron than to the trigonal prism. Accordingly, the $S(C_i)$ value, around 1.0, is about one half to that found for W sites in the **m-13** polymorph.

site		$d_{M\text{-}O}$ (Å)	S(OC)	S(TP)	S(COC)	S(CPT)	$S(C_i)$
W (4a)	exp.	1.921	1.074	11.010	-	-	1.033
	calc	1.951	1.117	10.944			1.074
Y1 (4a)	exp.	2.340	-	-	2.226	2.215	16.545
	calc.	2.332			2.273	2.221	16.453
Y2 (4a)	exp.	2.326	-	-	3.049	2.030	21.206
	calc	2.331			2.960	1.866	21.209

Table 2 Experimental[74] and optimized (PBEsol functional) structure for the coordination environment of Y^{3+} and W^{6+} in the monoclinic **o-19-z4** polymorph of Y_2WO_6. The $d_{M\text{-}O}$ values in the third column refer to average M-O (M = W or Y) distances for each polyhedron. Labels for reference polyhedra used in the shape analysis are the same as those in table 1.

According to the distribution of Y-O distances the two different sites occupied by Y^{3+} are heptacoordinate, with the smallest shape measure for the capped triangular prism, although a quite similar value is found for the capped octahedron in the case of the Y1 sites. Further analysis of the shape indicates that none of the structures lies on the interconversion path between the two polyhedra and, thus, the simplest description for all of them is that of a distorted capped triangular prism. The *S(C$_i$)* values indicate that the environment around the Y2 sites is much more asymmetric than that around the Y1 ones. The Y-O average distances are very similar to those found for the **m-13** polymorph.

Orthorhombic *P*2$_1$2$_1$2$_1$ (Z = 8) polymorph. A different orthorhombic polymorph, crystalizing also in the *P*2$_1$2$_1$2$_1$ (n. 19) spacegroup, but with eight formula units in the unit cell (Z = 8), has been reported by Beaury et al. for Y_2WO_6 at high temperatures [76, 77]. In this case (Fig. 3), yttrium ions are found at four different sites, three of them with eight-coordination (Fig.s 3b, c, and e) and the remaining one (Fig. 3d) with coordination number seven. Tungsten atoms occupy two different hexacordinated sites, one with a fairly regular octahedral shape (Fig. 3f) and the other one with a considerable distortion with respect to this ideal shape (Fig. 3g).

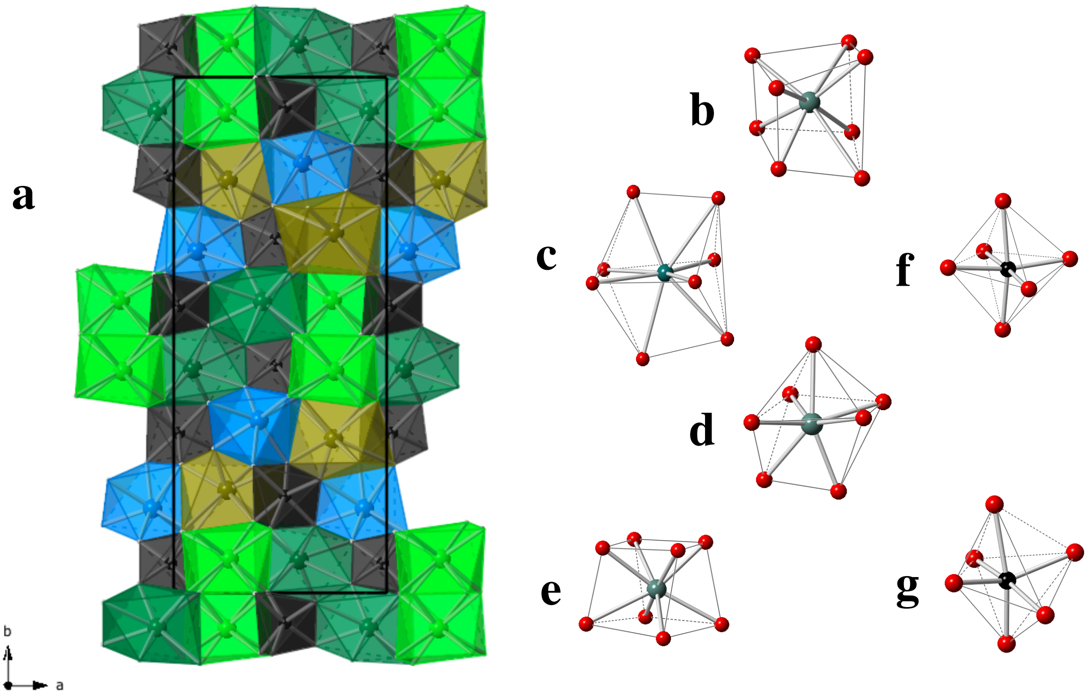

Fig. 3 Orthorhombic **o-19-z8** crystal structure for Y_2WO_6[77]. a) View of the complete structure along the crystallographic *c* axis highlighting the different coordination polyhedra: eight-coordinated Y atoms in different shades of green, seven-coordinated Y atoms in blue and W atoms in grey and black. b) Coordination environment for Y atoms in the Y1 sites, c) in the Y2 sites, d) in the Y3 sites, e) in the Y4 sites, d) for W atoms in the W1 sites and g) in the W2 sites.

All three functionals lead to quite similar structures, with the LDA functional yielding a somewhat smaller unit cell and the two GGA functionals slightly overestimating its volume (Table S3 in the supplementary material). The errors in the three cell parameters are also of the same magnitude in all three optimizations, indicating again that cohesive forces are very isotropic.

Information about the shape and symmetry of the coordination sphere for the W and Y atoms in the **o-19-z8** polymorph is given in table 3. As found for the other polymorphs, the size (estimated by the average M-O distances) and shape of the coordination polyhedra are quite well reproduced in the PBEsol optimized structure for all six different sites.

site		$d_{M\text{-}O}$ (Å)	S(OC)	S(TP)	S(COC)	S(CTP)	S(CU)	S(SAP)	S(TDD)	S(C_i)
W1 (4a)	exp.	1.984	1.016	12.188	-	-	-	-		0.881
	calc	1.956	1.354	10.591						1.249
W2 (4a)	exp.	1.900	5.030	7.572	-	-	-	-		3.853
	calc	1.965	5.359	7.551						4.653
Y1 (4a)	exp.	2.521	-	-	-	-	4.982	6.264	3.530	4.416
	calc.	2.460					4.541	5.916	3.171	4.074
Y2 (4a)	exp.	2.450	-	-	-	-	8.023	4.525	2.702	5.784
	calc	2.416					6.403	4.581	2.516	4.559
Y3 (4a)	exp.	2.263	-	-	1.471	3.091	-	-		19.946
	calc.	2.286			0.783	2.361				20.087
Y2 (4a)	exp.	2.366	-	-	-	-	1.981	6.555	3.757	1.664
	calc	2.364					1.598	6.778	3.929	1.412

Table 3 Experimental[77] and optimized (PBEsol functional) structure for the coordination environment of Y^{3+} and W^{6+} in the orthorhombic **o-19-z8** polymorph of Y_2WO_6. The $d_{M\text{-}O}$ values indicated in the third column refer to average M-O (M = W or Y) distances for each polyhedron. Labels for reference polyhedra used in the shape analysis are the same as those in table 1.

Two different coordination polyhedra are found for W in the **o-19-z8** polymorph (Figs. 3f and 3g). In both cases W atoms are surrounded by six O atoms with an average distance around 1.95Å, similar to those found for the other polymorphs. For W1 the smallest shape measure is for the octahedron, with a relatively small S(OC) value around 1.0, reflecting a moderate distortion along the minimal distortion path towards the trigonal prism (Bailar path)[75] with a generalized interconversion coordinate around 25%. The coordination environment for the W1 sites is thus very similar to that found for W atoms in the **o-19-z4** polymorph. As it can already be appreciated visually by comparing Figs. 3f and 3g, the local coordination environment at the W2 sites is also octahedral, but with a more sizeable departure from the ideal octahedral symmetry as reflected by the relatively high value for both S(OC) and $S(C_i)$. The main source of departure from the ideal octahedron in this case is not related to a Bailar twist but to the significant shortening of three out of the six W-O distances to approximately 1.8Å.

The distribution for the Y-O distances indicates that in the **o-19-z8** polymorph Y^{3+} is octacoordinated (Fig.s 3b, c, and e) in three sites while in the other one it is heptacoordinated. The average Y-O distances for the octacoordinated Y atoms are larger than for the heptacoordinated one, especially for sites Y1 and Y2. Shape analysis indicates that the coordination geometry at the Y1 and Y2 sites is best described by a distorted triangular dodecahedron. The $S(C_i)$ values in the range 4.0 - 5.0 for the two sites indicate however that departure from the ideal triangular dodecaedron (with inversion measure of 7.9) results in a noticeable increase of inversion symmetry. The coordination environment of Y atoms in the Y4 position (Fig. 3e) is best described by a cube and for those in the Y3 position by a capped octahedron.

Orthorhombic $P2_1ab$ polymorph. An alternative orthorhombic structure has been reported [42] for Y_2WO_6:Eu^{3+} phosphors. The monoclinic **m-13** phase was obtained via a conventional solid-state reaction, whereas a new orthorhombic **o-29** phase was found when using a facile, low-temperature combustion synthesis method. The X-ray powder diffraction pattern for this orthorhombic phase indicated that the Y_2WO_6:Eu^{3+} phosphors crystallized isostructurally with the Aurivillius Bi_2WO_6 phase, with the orthorhombic space group $P2_1ab$, (n. 29) [78]. This structure (Fig. 4) is layered, with perovskite-like WO_6 slabs and Bi^{3+} ions occupying sites with a highly asymmetric distorted pentagonal pyramidal geometry due to the presence of stereoactive $6s^2$ lone pairs on the Bi^{3+} cations (Figs. 4b and 4c).

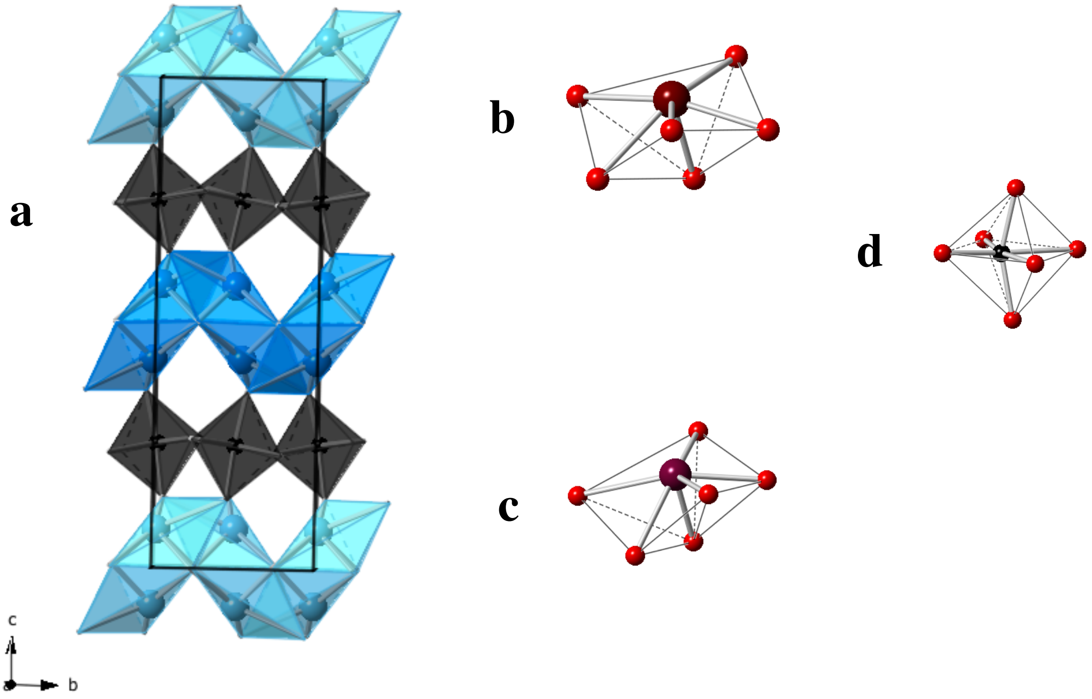

Fig. 4 Orthorhombic **o-29** crystal structure for Bi_2WO_6.[78] a) View of the complete structure along the crystallographic *a* axis highlighting the different coordination polyhedra: Bi atoms in different shades of blue and W atoms in black. b) Coordination environment for Bi atoms in the Bi1 sites, c) in the Bi2 sites, and d) for W atoms.

Since there is no available detailed structural information for the **o-29** Y_2WO_6 phase, we have optimized its crystal structure taking the isostructural low temperature Bi_2WO_6 Aurivilius phase as a starting point. As shown in table S4 in the supplementary material, optimization of the Bi_2WO_6 phase with the PBEsol functional yields a structure which is in good agreement with the experimental one, although due to the pronounced layered structure presented by this phase, the error in the estimation of the *c* lattice constant is significantly larger than those for *a* and *b*, leading to a slight overestimation of the cell volume.

Optimization of crystal structure for **o-29** Y_2WO_6 taking the experimental Bi_2WO_6 structure as an initial guess leads to a more compact Y_2WO_6 phase (Fig. 5) with a smaller cell volume, as it could be expected from the difference in ionic radii [79] between Bi^{3+} (1.03 Å) and Y^{3+} (0.9Å).

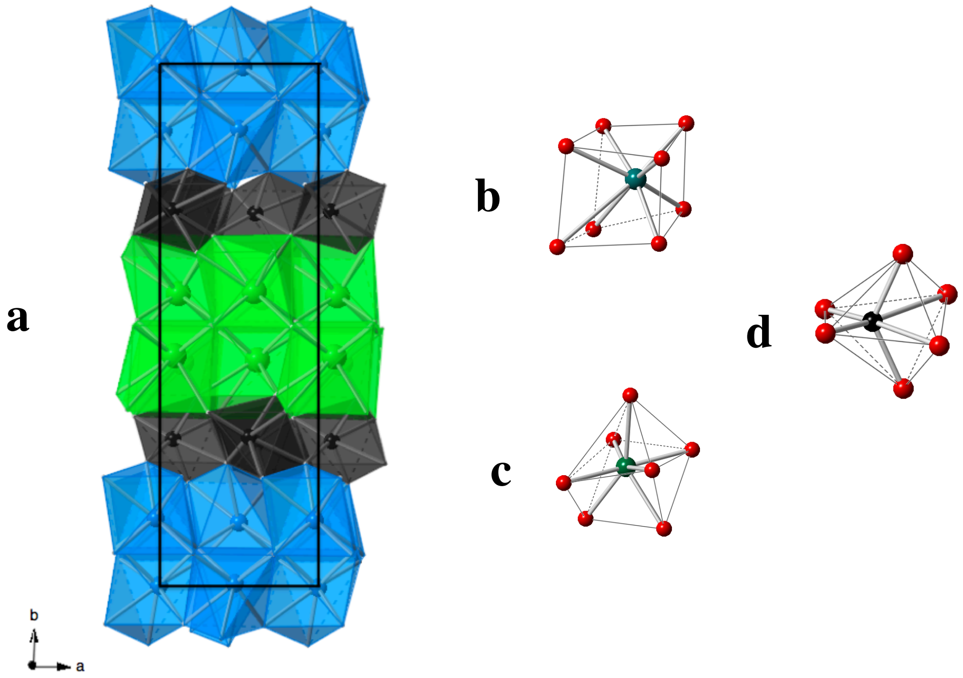

Fig. 5 Optimized (PBEsol functional) orthorhombic **o-29** crystal structure for Y_2WO_6. a) View of the full structure along the crystallographic *a* axis highlighting the different coordination polyhedra: Y1 atoms in green, Y2 ones in blue and W atoms in black. b) Coordination environment for Y atoms in the Y1 sites, c) in the Y2 sites, and d) for W atoms.

A simple visual comparison between the structures depicted in Figs. 4 and 5 shows that the principal effect of substituting Bi^{3+} by Y^{3+} is a compaction, especially in the Y-O layers, where a large restructuration has taken place. There are two different sites for Y in the final structure, one of them octacoordinated (Fig. 5b) and the other one heptacoordinated (Fig. 5c). According to the shape measures gathered in table 4, the best description for the octacoordinated Y1 site is that of a cube, and for the Y2 site that of a fairly regular capped octahedron. Accordingly, the $S(C_i)$ measure indicates a much larger departure from centrosymmetry for the heptacordinated Y2 site than for the octacordianted one. Sites occupied by W atoms can be described as distorted octahedra, with the departure from the ideal octahedral geometry being much more accused in the Y_2WO_6 case (Fig. 5 d) than in the Bi_2WO_6 one.

site	d_{M-O} (Å)	S(OC)	S(TP)	S(COC)	S(CTP)	S(CU)	S(SAP)	S(TDD)	S(C_i)
W	2.054	4.096	9.917	-	-	-	-	-	2.597
Y1	2.449	-	-	-	-	3.168	5.964	4.261	2.261
Y2	2.318	-	-	1.973	2.860	-	-	-	16.486

Table 4 Optimized structure of the coordination environment of W and Y atoms in the orthorhombic **o-29** polymorph of Y_2WO_6. The d_{M-O} values in the second column refer to average M-O (M = W or Y) distances for each polyhedron. Labels for reference polyhedra used in the shape analysis are the same as those in table 1.

Tetragonal *P*4*/nmm* polymorph. The last structure, **t-129**, described for phosphors based on Y_2WO_6 is tetragonal with space group *P*4*/nmm*, (n. 129). As reported in reference [70] Y_2WO_6 was prepared by a solid-state reaction of pure oxides, using NaCl as a mineralizer. The structural model given in reference [70] includes disorder, with half-occupancy for one of the oxygen sites. In this structure Y2 sites present a cubic coordination, while the actual coordination of the Y1 and W sites is unclear since it depends on the occupation of the O2 sites. In the ordered structure that we used for the optimization of the unit cell, both the W and the Y1 sites have trigonal prismatic coordination environments, but in reference [70] W and Y1 atoms are considered to be octacoordinated with square antiprismatic geometries, an unrealistic situation corresponding to a full occupation of the O2 sites.

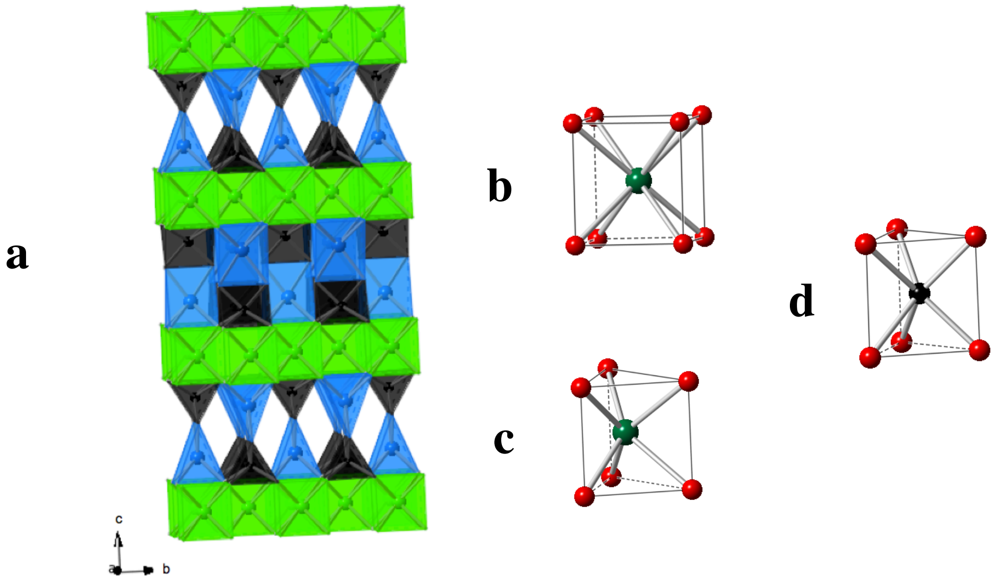

Fig. 6 Tetragonal **t-129** crystal structure for Y_2WO_6 considering an ideally ordered occupation of the O2 sites[70]. a) View of the complete structure along the crystallographic *a* axis highlighting the different coordination polyhedra: eight-coordinated Y atoms in bright green, seven-coordinated Y atoms in blue and W atoms in black. b) Coordination environment for Y atoms in the Y1 sites, c) in the Y2 sites, d) in the Y3 sites, and e) for W atoms.

Full optimization for this polymorph, considering an ordered structure where only half of the O2 sites are actually occupied, leads to a high energy structure with cell parameters in good agreement with those reported in reference [70]. In this case the estimated volume of the unit cell is practically the same as for the experimental structure, but this is just a fortuitous result due to a slight overestimation of the *a* parameter and a somewhat larger underestimation of the *c* parameter.

One of the sites occupied by yttrium in this structure, Y2, corresponds to a cubic coordination environment (Fig. 6b) while the other one, Y1, is hexacoordinated in the ordered structure considered in the optimization. The average Y-O distances for the octacoordinated Y atoms are similar to those found in other phases for either hepta or octaccoordinated Y, but those found for the hexacoordinate site are significantly longer than Y-O distances in the other phases, a fact that is probably due to the disordered nature of this position, for which the ordered average structure considered in our calculations does not result in an accurate description of the local environments in the real material. The shape analysis (table 5) indicates that the geometry around the Y2 atoms is highly symmetrical, with a very low shape measure for the cube, while that around the Y1 sites is that of a distorted trigonal prism. In the case of W, we find an unusual trigonal prismatic site, but this is also a consequence of adopting a regular structure in which oxygen atoms in the O2 sites are all arranged in ordered layers.

site		$d_{M\text{-}O}$ (Å)	S(OC)	S(TP)	S(CU)	S(SAP)	S(TDD)	S(C_i)
W (2c)	exp.	1.999	16.793	7.572	-	-	-	14.233
	calc	1.965	16.738	7.551				14.733
Y1 (2c)	exp.	2.521	18.818	3.029	-	-	-	16.892
	calc.	2.302	18.033	1.998				16.383
Y2 (2a)	exp.	2.368	-	-	0.272	11.028	7.938	0.000
	calc	2.364			0.142	11.032	7.975	0.095

Table 5 Optimized and experimental [70] structure of the coordination environment for Y^{3+} in the monoclinic **t-129** polymorph of Y_2WO_6. The $d_{M\text{-}O}$ values in the third column refer to average M-O (M = W or Y) distances for each polyhedron. Labels for reference polyhedra used in the shape analysis are the same as those in table 1.

3.2 Relative Stability

The monoclinic **m-13** polymorph is the stable bulk phase for pure Y_2WO_6 at ambient pressure and temperature conditions. The orthorhombic **o-19** and **o-19-z8** structures have been described as high temperature modifications, while the **o-29** and the **t-129** structures have only been described for rare earth containing phosphors based on Y_2WO_6, for which the larger volumes of the unit cell as compared to the one of the **m-13** polymorph could be a factor in stabilizing structures when Y is partially replaced by larger cations such as Eu^{3+}.

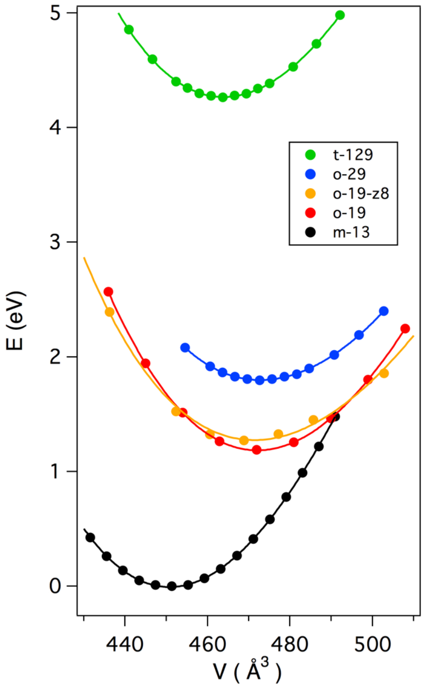

Fig. 7 Energy (PBEsol) vs volume curves for the different phases of Y_2WO_6 phases considered in this work. Energies and volumes correspond to unit cells containing 4 formula units. All energies are relative to that of the optimized structure corresponding to the lowest energy **m-13** polymorph.

Fig. 7 shows the energy versus volume curves obtained using the PBEsol functional for the five studied polymorphs. Strictly speaking, the absolute temperature should be considered as a variable for an assessment of the relative stability of the different phases, and hence, one should rely on free energies to understand why lattice parameters adopt certain values. The data presented in Fig. 7, obtained at 0K, may be nevertheless used qualitatively in this case to discuss the main trends in the structural stability for the different forms of Y_2WO_6.

As expected, the lowest calculated energy corresponds to the low temperature monoclinic **m-13** polymorph, which is about 0.3-0.5 eV per formula unit below the orthorhombic polymorphs. The energy for the tetragonal polymorph is considerably higher, more than 1 eV per formula unit above the **m-13** phase. This large difference, together with the large disorder in the occupation in the O2 position and the fact that it has only been described in just a single publication, makes us somewhat suspicious about the validity of the structural refinement reported in ref.[70]. The two $P2_12_12_1$ orthorhombic phases, **o-19-z4** and **o-19-z8**, have practically the same energy. They have been described either as high temperature polymorphs for pure Y_2WO_6 or as structures for rare earth doped phosphors. The larger equilibrium volumes and their relative low energies are in good agreement with these points. The third orthorhombic polymorph, **o-29**, has only been described for Er doped Y_2WO_6 phosphors. The equilibrium volume for this structure is similar to that of the other two orthorhombic phases and it is only slightly higher in energy, so that it seems a plausible structure, although a more precise structural refinement would be needed to fully confirm this hypothesis.

3.3 Electronic structure and bonding

According to our calculations (Figs. 8 and S1-S4) all five Y_2WO_6 polymorphs are wide gap insulators, with a calculated band-gap (PBEsol method) around 3 eV, somewhat below the experimental values in the range 3.2-3.4 eV reported for the **m-13** polymorph. This difference arises most probably from the well known trend of DFT to underestimate the band gap in semiconductors and insulators. Comparing the band-structures in Figs. 8 and S1-S4 the band-gap in the **o-19-z4** and **o-19-z8** phases is predicted to be similar to that found for the **m-13** polymorph, but significantly lower in the **o-29** (about 2.5 eV) and **t-129** polymorphs (about 2.0 eV).

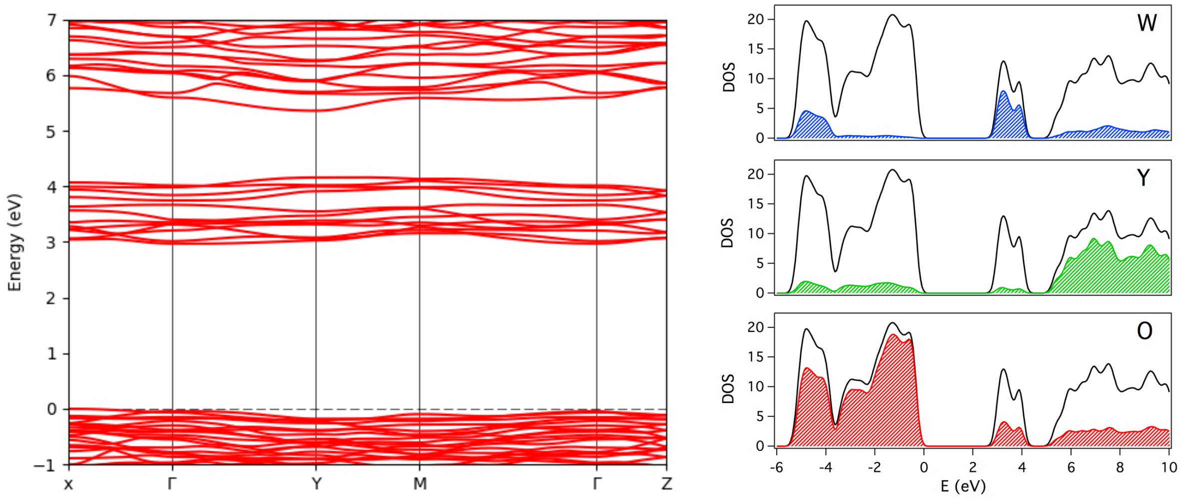

Fig. 8 (a) Band structure and (b) density of states calculated for the optimized structure of the **m-13** polymorph of Y_2WO_6 using the PBEsol method. The black curve in the DOS plots corresponds to the total density of states, while the shaded areas indicate the projections corresponding to W (blue), Y (green), and O (red) atoms. The origin of the energy scale has been shifted to make it coincide with the top of the valence band.

The basic features of the electronic structure of Y_2WO_6 are similar to those reported for other tungstates or molibdates such as scheelite ($CaWO_4$)[80] or wolframite ($ZnMoO_4$) [81]. The valence band (VB), mainly built from O_{2p} orbitals, is well separated from a quite narrow conduction band (CB) centred on the W_{5d} levels. Approximately 6 eV above the top of the VB we find a broad band with a large Y_{4d} contribution. In the **m-13** phase (Fig. 8) the W_{5d} centered CB, about 3 eV above the top of the VB (the origin of the energy scale in Fig. 8 has been set at the top of the VB), is quite narrow, about 1 eV, and it is well separated from the upper Y_{4d} centred band. The broad character of the Y_{4d} band, arising from a considerable mixture of Y orbitals with those on the surrounding O atoms, does not allow to clearly separate the contributions of the Y atoms in different coordination environments. Using this information, the origin of the luminescence observed for undoped Y_2WO_6 may be ascribed to the charge transfer transitions between O and W, although there is also an important extrinsic contribution to emission from possible defect states, for instance oxygen vacancies, generated when using different synthesis methods, annealing temperatures, or atmospheres [82].

The principal differences in the electronic structure between the polymorphs of Y_2WO_6 (Figs. 8 and S1-S4) are found in the W centred CB. This band is quite narrow in the **m-13** as well as in the two **o-19** polymorphs (~1eV), while polymorphs it is found to be considerably broader for both high energy **o-29** and **t-129** polymorphs. As a consequence, it leads to the narrowing of the band-gap as described above, and to its overlap with the broad Y centred band. These features are, however, not expected to raise any noticeable qualitative differences in the emission spectra for the different polymorphs besides the shift associated with the diminution of the band gap.

An interesting question regarding the possible preference in substituting Y^{3+} for rare earth cations is that of the local ionicity of the alternative coordination sites. In table S6 in the supplementary material we have gathered the net charges calculated for W and Y atoms in all five studied polymorphs as obtained from a Mulliken population analysis. Although, due to well known shortcomings such as the basis set dependence, Mulliken charges should be taken with caution, comparison between different compounds may reveal interesting trends in the electronic structure and its relation with structural features. In this case, the values for the charges obtained for Y in all phases are quite similar, lying in a relatively narrow range comprised between +1.25 and +1.49. These values are larger than those found in other yttrium compounds commonly used as hosts for rare-earth based phosphors such as Y_2O_3 (Q_Y = +1.18, +1.21) and Y_2O_2S (Q_Y = +1.21)[45] indicating a fairly larger degree of ionicity for the Y-O interactions in Y_2WO_6.

Although there is no net correlation between the average distance and the calculated net charge of Y atoms in the different coordination sites, as a general trend we can notice that octacoordinated sites present a lower charge (lower ionicity) than heptacoordinated ones, or in other words, Y-O interactions are expected to have a higher covalent character, with a larger degree of orbital mixing, in octacoordinated sites.

Mulliken charges calculated for the W atoms are found in a very narrow range, +2.12 to +2.26, as could be expected since WO_6 octahedra are found to be very similar in all studied phases. The relatively low value for the charge (the formal charge of W in Y_2WO_6 is +6) is indicative of a considerable covalent bonding within the WO_6 units, as it can be appreciated in the DOS plot in fig. 8b, where a sizeable participation of W_{5d} atomic orbitals involved in W-O bonding can be found in the region approximately 5 eV below the Fermi level.

3.4 Optical properties

The main aim of this work is to gain some information on the physical properties of a series polymorphs of Y_2WO_6 that have been used as host materials in inorganic phosphors. For this reason, their optical properties are the among the most important features towards possible applications. In the previous section we have already discussed the electronic structure around the band gap, for which a calculated value around 3eV is found for the low energy monoclinic and orthorhombic polymorphs. The principal feature modulating the band gap is the W_{5d} centred band that appears between the top of the mainly O_{2p} valence band and the bottom of the broad empty Y_{4d} band. It is precisely due to the presence of this W_{5d} band that the values of the band gap (3.0 eV calculated, 3.2-3.4 eV experimental for the **m-13** polymorph) are significantly lower than those found [45] for Y_2O_3 (4.1 eV calculated, 5.0 - 6.0 eV experimental) or Y_2O_2S (2.9 eV calculated, 4.6 - 4.9 eV experimental band gap), another Y containing material widely used as host for rare-earth based phosphors, although in this case the lower value for the gap in comparison to Y_2O_3 is mainly due to the stronger covalent character of Y-S interactions that leads to a broadening of both valence and conduction bands. A case similar to Y_2WO_6, where the gap is modulated by the presence of a non Y-centred band was found for Y_2TeO_6 (3.3 eV calculated band gap) [45].

Besides the optical gap we have also calculated the real and imaginary parts of the dielectric function, $\varepsilon_1(\omega)$ and $\varepsilon_2(\omega)$, for all polymorphs (Figs. 9 and S5-S7). For the **m-13** phase, the imaginary part of the dielectric function, ε_2, shows a sharp edge at approximately 3 eV giving rise to a relatively narrow peak arising from transitions between the valence O_{2p} band and the lowest empty, mostly W_{5d} band. This peak, which is associated to the characteristic charge-transfer transitions observed in undoped Y_2WO_6 [17], is clearly separated from the broad peak around 9 eV due to excitations to the Y_{4d} centred bands and it should be easily identified in an absorption spectrum. The broad peak due to Y_{4d} centred bands is similar to that found in the dielectric function calculated for c-Y_2O_3,[45] although in this case it is slightly shifted (~2 eV) towards higher energies, a shift that is indicative of the fairly larger degree of covalent character for the Y-O interactions in Y_2O_3 as discussed above.

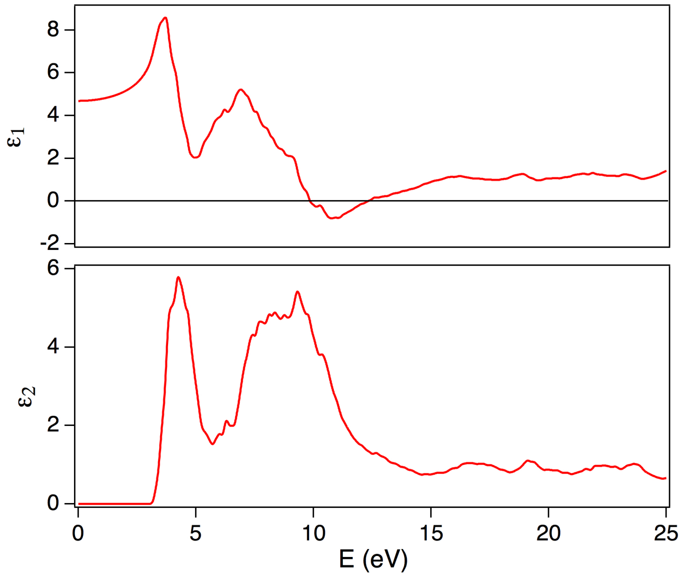

Fig. 9 Real (ε_1) and imaginary (ε_2) parts of the dielectric function calculated for the optimized structure of the **m-13** polymorph of Y_2WO_6 (PBEsol functional).

As expected from the calculated band structure, the calculated dielectric functions for the other polymorphs of Y_2WO_6 are quite similar, especially for the **o-19** phases for which the sharp peak due to excitations to the W_{5d} bands is also clearly visible. For the higher energy **o-29** and **t-129** polymorphs the W_{5d} bands partially overlap with the broader Y_{4d} centred bands and the sharp peak appears now only as a shoulder to the broader Y_{4d} peak. These results suggest that the appearance of the peak associated to the W_{5d} bands in the absorption spectrum of undoped samples of Y_2WO_6 could be an additional clue to the determination of the dominant polymorph in poorly crystalline samples.

The values calculated for the electronic contribution to the static dielectric permittivity are very similar for all five polymorphs, lying in the range ε^{∞} = 4.85 - 4.40. From these values an estimated refraction index of about 2.1 - 2.2 is expected for Y_2WO_6 in any of the described phases. The value calculated for ε^{∞} is significantly larger than those found previously for Y_2O_3 (3.65) or Y_2TeO_6 (3.68), but in the same range as that found for the more covalent compound Y_2O_2S (4.7) [45].

3.5 Site preference for doping

The ionic radii of the trivalent lanthanides (e.g. 1.07 Å for Eu^{3+}) is quite similar to that of Y^{3+} (1.02 Å) and much larger than the ionic radius of W^{6+} (0.60 Å)[79]. Therefore, upon doping, lanthanide ions are expected to replace preferentially Y^{3+} ions. In a given polymorph, Ln^{3+} ions can substitute Y^{3+} in any of the different crystallographic sites. Since the resulting luminescence will be strongly affected by the coordination environment around the dopant atom it is interesting to study if there are some preferences for doping at some particular sites and how the local crystal structure is deformed upon replacement of Y^{3+} by Ln^{3+}. For this purpose we have performed calculations in which one of the eight Y^{3+} ions in the Z=4 unit cell of the **m-13**, **o-19-z4**, **o-29**, and **t-129** polymorphs has been replaced by an Eu^{3+} ion. In the case of the **o-19-z8** polymorph, only one of the 16 Y^{3+} ions in the Z=8 unit cell has been replaced. This leads to an $Y_{2-x}Eu_xWO_6$ stoichiometry with x = 0.25 for the polymorphs with Z=4 cells and x=0.125 for the **o-19-z8** phase. These concentrations of Eu^{3+} ions are not uncommon in experimental data found in the literature, where the synthesis of phosphors with *x* values between 0 and 0.4 has been reported.

In all cases, one Y^{3+} ion has been replaced by one Eu^{3+} ion in the PBEsol optimized structure of Y_2WO_6 to calculate a first approximation (initial) to the substitution energy (for the Z = 4 case):

$$E_{in}(eV) = E(EuY_7W_4O_{24}) + E(Y^{3+}) - E(Y_8W_4O_{24}) - E(Eu^{3+})$$

In a second stage, the doped structure has been further relaxed without any restriction to study the local structural changes induced by substitution at a given Y^{3+} site. The total insertion energy (relaxed) is then obtained by an analogous equation, where the energy $E(EuY_7W_4O_{24})$ corresponds now to that of the relaxed structure.

In the following we will describe first the results obtained for each polymorph, to end with a discussion of the general trends that emerge when considering all cases together. Since the **m-13** polymorph is the most abundant one in the literature, we will describe the effects of the Eu substitution on the electronic structure only for this polymorph, although the findings are quite general and similar conclusions can be reached for the other cases.

Monoclinic *P*2/*c* polymorph. As discussed earlier, there are three non-equivalent Y sites in the monoclinic (**m-13**) structure of Y_2WO_6, one of them with coordination number 7 and the other two with coordination number 8. As shown in table S7 in the supplementary material, replacing an Y^{3+} ion for an Eu^{3+} one without relaxing the structure costs about 6 eV and this value is reduced to about 3.5 eV when the structural relaxation is been taken into consideration. In all three cases relaxation of the structure results in an enlargement of the coordination sphere around the Eu atom, with an increase of about 0.2Å in the average M-O distance. Taking a look at the changes in the shape and symmetry measures in table S7, where no extraordinary changes are observed, it is evident that upon relaxation the increase in the average size of the coordination environment is quite isotropic, preserving the main geometric features of the coordination site.

According to our calculations, the preferred site for Eu substitution in the **m-13** polymorph is at the octacoordinated Y2 site, with an insertion energy about 0.5 eV lower than for the other two sites. This finding is in agreement with the interpretation given by van Noort and Popma of their ^{151}Eu Mössbauer spectroscopy measurements indicating that at low Eu concentrations substitution takes place preferentially at the octacoordinated sites[83]. Notice that, although substitution at the octacoordinated Y2 site is preferred, in this case it costs practically the same energy to introduce Eu in an octacoordinated Y1 or heptacoordinated Y3 site, so that, apparently, the coordination number is not a determining factor to decide a priori where substitution will take place preferentially. More on this issue will be discussed at the end of the section when comparing insertion energies between different polymorphs.

Orthorhombic *P*2$_1$2$_1$2$_1$ (Z = 4) polymorph. The orthorhombic **o-19-z4** structure has Y^{3+} ions in two distinct heptacoordinated crystallographic positions and the calculated insertion energies (table S8 in the supplementary material) are similar for the two cases. The absolute values are similar than those found for the **m-13** polymorph: substitution of Y by Eu costs about 6 eV per ion, a value that is reduced to about 3.5 eV when the structure is allowed to relax. As shown by the average M-O distance, the size of the two sites is similar, and relaxation leads also in this case to an isotropic expansion with the average M-O distance increasing by about 0.3Å. Since the magnitude of the insertion energy is mainly dictated by the necessary expansion of the coordination sphere, in this case the insertion energies for the two sites are quite close and our results suggest that for this polymorph no preferential substitution should be expected.

Orthorhombic $P2_12_12_1$ (Z = 8) polymorph. The orthorhombic **o-19-z8** polymorph has been described as a high temperature phase for Y_2WO_6 as well as for doped phases with different amounts of rare earth ions substituting Y. As expected for a high temperature polymorph, it has a higher molar volume (see Fig. 7) which is clearly reflected in the average Y-O distances of the first two octaccordinated sites, which are about 0.1Å larger than those found in the previous phases. Accordingly, we find that insertion of Eu in this phase (table S9, supplementary material) is on average easier than in the monoclinic **m-13** polymorph, especially in either the Y1 or Y2 positions (about 3 eV after relaxation). Insertion in the other two sites (about 4 eV after relaxation) implies a higher energy cost, a finding that can be easily rationalized taking into account their smaller volumes as evidenced by the corresponding average Y-O distances. Note also that for this phase, apparently almost no energy is consumed in relaxing the structure for insertion in any of the four Y sites, although the expansion of the average M-O distances is of the same order of that found for other polymorphs. This behaviour is related to the fact that in this case we are substituting only one out of each 16 Y atoms in the unit cell, and consequently, a much smaller restructuration of the structure is needed to absorb the volume increase induced by the replacement of one Y^{3+} cation by a larger Eu^{3+} one.

From the insertion energies calculated for this polymorph we expect a preferential substitution into the Y1 and Y2 sites, although Eu^{3+} is predicted to occupy these two octacoordinated sites with a similar probability.

Orthorhombic $P2_1ab$ polymorph. The orthorhombic **o-29** polymorph has Y in two distinct sites, one of them octa- and the other one heptacoordinated. The size of the first is somewhat larger, and accordingly the insertion energy for Eu^{3+} (table S10, supplementary material) is slightly lower, although the differences, 3.2 vs 3.5 eV are not large enough to suggest a preferential substitution.

Tetragonal *P4/nmm* polymorph. As discussed previously, there are two very different coordination sites for Y in the **t-129** polymorph one of them (Y2) with a practically cubical geometry and the other one (Y1) with an uncommon triangular prismatic geometry. As seen in table S11 in the supplementary material it is apparently much easier to introduce Eu in the trigonal prismatic Y1 sites, with an insertion energy about 2.7 eV per Eu^{3+} cation, much lower than the 4 eV found for the octahedral sites. The fact that the average Y-O distances are similar before and after Eu^{3+} substitution, leads us to the conclusion that for this case the coordination geometry rather than the size of the site is the determining factor. From our calculated insertion energies we may predict a preferential substitution for this polymorph, with Eu^{3+} cations replacing mostly Y^{3+} in the trigonal prismatic Y1 sites. Note, however, that as mentioned above, the actual crystal structure considered in our calculations is just an ordered model where the large number of O vacancies in the structure has been distributed in a precise fashion, leading to a coordination geometry which may be quite different from that in a structure with a different ordering of O vacancies leading to a higher average coordination around the Y^{3+} cations in the Y1 sites.

General trends. In Fig. 10 we have plotted the insertion energy (after relaxation) as a function of the average Y-O distance for all Y sites in the five polymorphs. If we disregard the unusual six-fold trigonal prismatic Y1 site in the **t-129** polymorph (green point) with an unexpected low insertion energy, the general trend evidenced in Fig. 10 is that the major factor determining the insertion energy is the size of the site where substitution takes place. Accordingly, it is easier to replace Y^{3+} by Eu^{3+} in the larger sites, and since increasing the coordination number results in a larger size for the coordination site, it is, in general, easier to insert Eu^{3+} in octa- than in heptacoordinated sites. Although this is the general trend, the actual coordination geometry is nevertheless important, and in cases with intermediate sized coordination sites (with average Y-O distances around 2.35Å) it is apparently easier to insert Eu^{3+} in heptacoordinated sites than in octacoordinated ones.

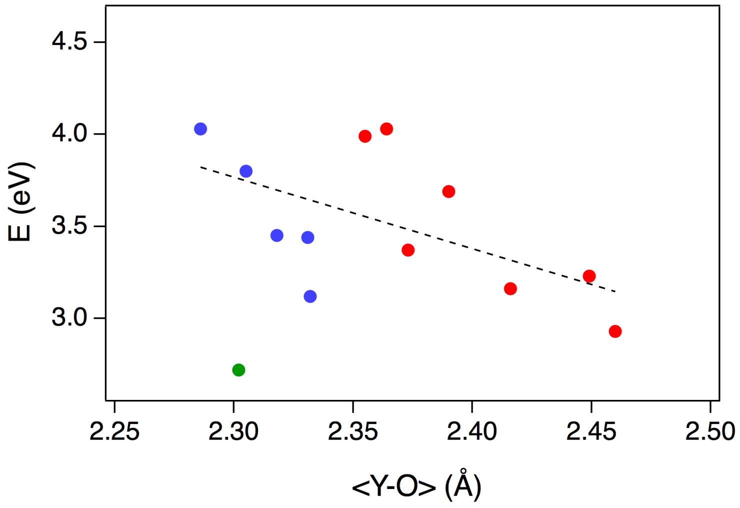

Fig. 10 Insertion energy (after structural relaxation) in eV per Eu^{3+} atom as a function of the average Y-O distance (Å) of the size of the Y site in the optimized Y_2WO_6 structure. Green dots:

hexacoordinated sites, blue dots: heptacoordinated sites, and red dots: octacoordinated sites. The dashed line corresponds to a linear fit of the data (excluding the case of the hexacoordinated Y1 site in the **t-129** polymorph) and is meant only as a guide to the eye to highlight the general trend of the insertion energy versus the size of each individual site.

The apparently favourable substitution into the hexacoordinated Y1 site in the **t-129** polymorph does not follow the general trend. This result should, however, be taken with some caution due to the particularities of the **t-129** structure discussed in earlier sections. Since this structure has only been proposed in one of the multiple works devoted to Y_2WO_6 based rare-earth containing phosphors[70], we think that there is still not enough evidence to consider it as an undisputed alternative to the lower energy structures proposed in other works.

As far as the symmetry of the coordination sites is concerned, we have found that, in general, substitution will take place preferentially in the larger octacoordinated sites and these have, as expected, smaller deviations from centrosymmetry (smaller $S(C_i)$ values), especially when they correspond to slightly distorted cubic geometries. Easy insertion in a highly asymmetric heptacoordination site is, however, possible in the case of the **o-19-z4** polymorph, which is in this respect a desirable target for obtaining efficient phosphors by doping with rare earths.

Let us note that the actual structure for the Y_2WO_6:Eu^{3+} phosphors will change with the contents of Eu^{3+}. In this respect our calculations have been done adopting the simplest possible models, that is, substituting only one Y^{3+} ion for Eu^{3+} in the unit cell. As discussed above, the concentration of Eu^{3+} in these models is reasonable when compared to the experimental one, although it is in the high range of experimental values. Analysis of samples with lower concentrations would require the use of larger models (larger supercells) which result in too costly calculations that we cannot perform with our actual equipment. Another interesting question that is also out of reach with our computational facilities at present is that of the possibility of clustering of Eu^{3+} ions in the structure and if this segregation would affect the optical properties of the phosphor. To address this issue it is, however, necessary to use models with quite large supercells and to perform an unreasonable number of calculations to sample all possible distributions of two or various Eu^{3+} ions within the supercell and assess their relative stabilities. In this respect the calculations presented in this work are just based on the simplest possible models of Eu^{3+} substitution in Y_2WO_6, and the information obtained, although valuable, does not cover all possible issues of the doping process. Work exploring this type of questions for a simpler system, Er^{3+} doped $BaTiO_3$ phosphors, using empirical force-fields to simulate the large supercells needed in this type of studies is on the way in our laboratory and if successful, we expect to apply this alternative approach to more complex systems such as Y_2WO_6:Eu^{3+} phosphors.

4. Conclusions

In this work we have undertaken a thorough computational study by first principles DFT-based electronic structure methods of the five polymorphs of Y_2WO_6 that have been previously described in the literature. Optimization of the crystal structures yields results in good agreement with those determined experimentally by X-ray diffraction, both for the cell parameters as well as for the local environments for each of the Y atoms in different crystallographic positions, although some questions about the validity of a tetragonal structure suggested for Y_2WO_6:Ln^{3+} phosphors remain open. The monoclinic *P*2/*c* (**m-13**) phase is predicted to be the most stable one at ambient conditions, although high temperature orthorhombic phases with larger molar volumes could be favoured upon replacement of some Y^{3+} cations by larger Ln^{3+} ones such as Eu^{3+}, and hence, provide plausible structures for Y_2WO_6:Ln^{3+} phosphors at ambient conditions.

The electronic structures calculated for all five suggested polymorphs are qualitatively similar, with the top of the valence band dominated by the O_{2p} orbitals and a relatively narrow WO_6-centred conduction band below a broad Y_{4d} centred band. The calculated band-gap around 3eV calculated for the most common monoclinic **m-13** polymorph is somewhat below the reported experimental values in the range 3.2-3.4 eV, as expected for DFT-based calculations that tend to underestimate this magnitude.

Insertion energies for Eu^{3+} cations replacing Y^{3+} in the different polymorphs are estimated to be in the range of 3 - 4 eV per cation, with the smaller values corresponding to substitutions into the generally larger octacoordinated Y^{3+} sites. According to our calculations, the preferred site for Eu^{3+} substitution in the most common **m-13** polymorph is at the octacoordinated Y2 site, with an insertion energy about 0.5 eV lower than for the other two sites, a finding that is in agreement with ^{151}Eu Mössbauer spectroscopy measurements that have been interpreted considering that at low Eu concentrations substitution takes place preferentially at the octacoordinated sites.

Acknowledgement

This work was supported by Ministerio de Ciencia, Innovación y Universidades - Spain (Project PGC2018-093863-B-C22), by the Maria de Maeztu Units of Excellence Program under Grant MDM-2017-0767, Generalitat de Catalunya (2017SGR1289), and FONDECYT-Chile (Project 1181302). PA gratefully acknowledges the *Universidad Católica del Norte* (VRIDT) for the warm hospitality and financial support received during his stay in Antofagasta.

References

[1] L. Chen, C.C. Lin, C.W. Yeh, R.S. Liu, Light Converting Inorganic Phosphors for White Light-Emitting Diodes, Materials 3 (2010) 2172-2195.

[2] W. Ran, H.M. Noh, B.C. Choi, S.H. Park, J.H. Kim, J.H. Jeong, J. Shi, G. Liu, Eu^{3+} doped (Li, Na, K) $LaMgWO_6$ red emission phosphors: An example to rational design with theoretical and experimental investigation, J. Alloys Compd. 785 (2019) 651-659.

[3] B. Zhang, J. Zhang, Y.Y. Guo, J. Wang, J. Xie, X. Li, W. Huang, L. Wang, Q. Zhang, Synthesis and photoluminescence of double perovskite $La_2LiSbO_6:Ln^{3+}$ (Ln= Eu, Tb, Tm, Sm, Ho) phosphors and enhanced luminescence of $La_2LiSbO_6:Eu^{3+}$ red phosphor via Bi^{3+} doping for white light emitting diodes, J. Alloys Compd. 787 (2019) 1163-1172.

[4] K. Naveen Kumar, L. Vijayalakshmi, J. Choi, J. Su Kim, Efficient red-luminescence of $CaLa_2ZnO_5$ phosphors co-doped by Ce^{3+} and Eu^{3+}, J. Alloys Compd. 787 (2019) 711-719.

[5] S. Bai, Y. Liu, G. Tan, H. Ren, D. Liu, K. Wang, R. Wang, Y. Zhu, S. Ye, Novel multi-wavelength effectively excited $ZnWO_4$-$WO_3:Eu^{3+}$ multiphase red phosphor for white light-emitting diodes, J. Alloys Compd. 807 (2019) 151668.

[6] M. Xia, Z. Ju, H. Yang, Z. Wang, X. Gao, F. Pan, W. Liu, Red-emitting enhancement by inducing lower crystal field symmetry of Eu^{3+} site in $CaWO_4:Eu^{3+}$ phosphor for n-UV w-LEDs, J. Alloys Compd. 739 (2018) 439-446.

[7] M. Rajendran, S. Vaidyanathan, New red emitting phosphors $NaSrLa(MO_4)_3:Eu^{3+}$ [M = Mo and W] for white LEDs: Synthesis, structural and optical study, J. Alloys Compd. 789 (2019) 919-931.

[8] C. Liu, Z. Zhou, Y. Zhang, Synthesis and luminescence properties of novel red-emitting $Na_2ZnSiO_4:Eu^{3+}$ phosphor with intense $^5D_0/^7F_4$ transition and high quantum yield, J. Alloys Compd. 787 (2019) 1158-1162.

[9] Y. Hua, J.S. Yu, Broadband near-ultraviolet excited $La_2Mo_2O_9:Eu^{3+}$ red-emitting phosphors with high color purity for solid-state lighting, J. Alloys Compd. 783 (2019) 969-976.

[10] R. Cao, T. Chen, Y. Ren, T. Chen, H. Ao, W. Li, G. Zheng, Synthesis and photoluminescence properties of $Ca_2LaTaO_6:Mn^{4+}$ phosphor for plant growth LEDs, J. Alloys Compd. 780 (2019) 749-755.

[11] J. Zhang, C. Jin, Electronic structure, upconversion luminescence and optical temperature sensing behavior of Yb^{3+}-Er^{3+}/Ho^{3+} doped $NaLaMgWO_6$, J. Alloys Compd. 783 (2019) 84-94.

[12] Y. Zhu, Q. Meng, W. Sun, S. Lü, Sm^{3+}, Tb^{3+} co-doped $NaLa(MoO_4)_2$ temperature sensing materials based on the fluorescence intensity ratio, J. Alloys Compd. 784 (2019) 456-462.

[13] K. Li, R. Van Deun, Site-Bi^{3+} and Eu^{3+} dual emissions in color-tunable $Ca_2Y_8(SiO_4)_6O_2$:Bi^{3+}, Eu^{3+} phosphors prepared via sol-gel synthesis for potentially ratiometric temperature sensing, J. Alloys Compd. 787 (2019) 86-95.

[14] W.M. Yen, S. Shionoya, H. Yamamoto, Phosphor Handbook, 2nd Edition, CRC Press, Boca Ratón, USA, 2007.

[15] V.A. Efremov, Characteristic features of the crystal chemistry of lanthanide molybdates and tungstates, Russ. Chem. Rev. 59 (1990) 627-642.

[16] A.M. Kaczmarek, R. Van Deun, Rare earth tungstate and molybdate compounds – from 0D to 3D architectures, Chem. Soc. Rev. 42 (2013) 8835-8848.

[17] G. Blasse, The Luminescence of Closed-shell Transition-metal Complexes. New Developments, Structure and Bonding 42 (1980) 1-41.

[18] L. Tian, P. Yang, H. Wu, F. Li, Luminescence properties of Y_2WO_6:Eu^{3+} incorporated with Mo^{6+} or Bi^{3+} ions as red phosphors for light-emitting diode applications, J. Lumin. 130 (2010) 717-721.

[19] Q. Wang, Z. Ci, G. Zhu, S. Xin, W. Zeng, M. Que, Y. Wang, Multicolor bright Ln^{3+} (Ln = Eu, Dy, Sm) activated tungstate phosphor for multifunctional applications, Opt. Mat. Express 4 (2013) 142-154.

[20] F.B. Xiong, D.S. Guo, H.F. Lin, L.J. Wang, H.X. Shen, W.Z. Zhu, High-color-purity red-emitting phosphors RE_2WO_6:Pr^{3+} (RE = Y, Gd) for blue LED, J. Alloys Compd. 647 (2015) 1121-1127.

[21] X. Shi, J.-G. Li, Q. Zhu, X. Li, X. Sun, Hydrothermal assisted synthesis and photoluminescence of $(Y_{1-x}Eu_x)_2WO_6$ red phosphors, J. Alloys Compd. 695 (2017) 1984-1992.

[22] H. Quian, J. Zhang, L. Yin, Crystal structure and optical properties of white light-emitting Y_2WO_6:Sm^{3+} phosphor with excellent color rendering, RSC Advances 3 (2013) 9029-9034.

[23] Z. Mu, Y. Hu, L. Chen, X. Wang, G. Ju, Z. Yang, Y. Jin, A single-phase, color-tunable, broadband-excited white light-emitting phosphor Y_2WO_6: Sm^{3+}, J. Lumin. 146 (2014) 33-36.

[24] R. Van Deun, D.H. Ndagsi, J. Liu, I. Van Driessche, K. Van Hecke, A.M. Kaczmarek, Dopant and excitation wavelength dependent color-tunable white light-emitting Ln^{3+}: Y_2WO_6 materials (Ln^{3+} = Sm, Eu, Tb, Dy), Dalton Trans. 44 (2015) 15022-15030.

[25] F.B. Xiong, C.Y. Han, H.F. Lin, Y.P. Wang, H.Y. Lin, H.X. Shen, W.Z. Zhu, White light emission from novel host-sensitized single-phase Y_2WO_6: Ln^{3+} (Ln^{3+} = Eu^{3+}, Dy^{3+}) phosphors, Ceram. Int. 42 (2016) 13841-13848.

[26] P. Hu, W. Zhang, Z. Hu, Z. Feng, L. Ma, X. Zhang, X. Sheng, L. Luo, Y. Wang, Luminescence and cathodoluminescent properties of monoclinic Y_2WO_6 co-doped with Dy-Bi, Mod. Phys. Lett. B 31 (2017) 1750182.

[27] U. Farooq, Z. Zhao, Z. Sui, C. Gao, R. Dai, Z. Wang, Z. Zhang, $Tm^{3+}/Dy^{3+}/Eu^{3+}$ (Sm^{3+}) tri-activated Y_2WO_6 as one potential single-phase phosphor for WLEDs, J. Alloys Compd. 778 (2019) 942-950.

[28] A.K. Soni, V.K. Rai, Intrinsic optical bistability and frequency upconversion in Tm^{3+}-Yb^{3+}-codoped Y_2WO_6 phosphor, Dalton Trans. 43 (2014) 13563-13570.

[29] X. Gao, D. Xu, J. Du, Z. Yang, J. Sun, Luminescence properties of Y_2WO_6:Yb^{3+}/Er^{3+} with enhanced red emission via upconversion, J. Rare Earths 35 (2017) 1065-1070.

[30] X. Gao, D. Xu, Y. Zhu, Z. Yang, J. Du, J. Sun, Up-Conversion Luminescence Properties of Ho^{3+} Doped and Yb^{3+}/Ho^{3+} Co-Doped Y_2WO_6 Phosphors, Key Eng. Mat. 727 (2017) 618-622.

[31] C. Chen, P. Cai, L. Qin, J. Wang, Y. Huang, H.J. Seo, Hydrothermal synthesis and upconversion luminescence of Y_2WO_6:Yb^{3+}/Er^{3+} crystals, J. Alloys Compd. 747 (2018) 803-808.

[32] M.N. Huang, Y.Y. Ma, F. Xiao, Q.Y. Zhang, Bi^{3+} sensitized Y_2WO_6:Ln^{3+} (Ln = Dy, Eu, and Sm) phosphors for solar spectral conversion, Spectrochim. Acta A 120 (2014) 55-59.

[33] A.K. Soni, Stark sublevels investigation in Y_2WO_6:Tm^{3+}-Yb^{3+} phosphor for thermometry and internal temperature measurement, Mater. Res. Express 5 (2018) 055016.

[34] J. Wang, Y. Bu, X. Wang, H.J. Seo, Optical thermometry in low temperature through manipulating the energy T transfer from WO_6^{6-} to Ho^{3+} in Y_2WO_6:Ho^{3+} phosphors, Opt. Mat. 84 (2018) 778-785.

[35] J. Zhang, B. Ji, G. Chen, H. Z., Upconversion Luminescence and Discussion of Sensitivity Improvement for Optical Temperature Sensing Application, Inorg. Chem. 57 (2018) 5038-5047.

[36] J. Wang, Z.-J. Zhang, J.-T. Zhao, H.-H. Chen, X.-X. Yang, Y. Tao, Y. Huang, Luminescent metastable Y_2WO_6:Ln^{3+} (Ln = Eu, Er, Sm, and Dy) microspheres with controllable morphology via self-assembly, J. Mater. Chem. 20 (2010) 10894-10900.

[37] R. Hao, Q. Meng, W. Liu, H. Liu, Synthesis and luminescent properties of Eu^{3+} doped Y_2WO_6 nanophosphors, J. Rare Earths 31 (2013) 864-869.

[38] A.M. Kaczmarek, K. Van Hecke, R. Van Deun, Enhanced Luminescence in Ln^{3+}-Doped Y_2WO_6 (Sm, Eu, Dy) 3D Microstructures through Gd^{3+} Codoping, Inorg. Chem. 53 (2014) 9498-9508.

[39] H. Gao, Y. Bai, J. Zhang, Z. Tang, Microsphere morphology tuning and photo-luminescence properties of monoclinic Y_2WO_6, J. Cryst. Growth 416 (2015) 148-153.

[40] J. Li, Z. Wu, X. Sun, X. Zhang, R. Dai, J. Zuo, Z. Zhao, Controlled hydrothermal synthesis and luminescent properties of Y_2WO_6:Eu^{3+} nanophosphors for light-emitting diodes, J. Mater. Sci. 52 (2017) 3110-3123.

[41] W.-F. Rao, Y. Guan, J.-Y. Yang, Q.-Q. Huang, J.H. Miao, Fabrication, characterization, and luminescent properties of Y_2WO_6: Gd^{3+}, Dy^{3+} hierarchical microspheres, J. Mat. Sci: Materials in Electronics 30 (2019) 4393 - 4399.

[42] J. Llanos, D. Olivares, V. Manríquez, D. Espinoza, I. Brito, Synthesis and luminescent properties of two different Y_2WO_6:Eu^{3+} phosphor phases, J. Alloys Compd. 628 (2015) 352-356.

[43] J. Llanos, D. Espinoza, R. Castillo, Energy transfer in single phase Eu^{3+}-doped Y_2WO_6 phosphors, RSC Advances 7 (2017) 14974-14980.

[44] J. Llanos, I. Brito, D. Espinoza, R. Sekar, P. Manidurai, A down-shifting Eu^{3+}-doped Y_2WO_6/TiO_2 photoelectrode for improved light harvesting in dye-sensitized solar cells, R. Soc. Open Sci. 5 (2018) 171054.

[45] P. Alemany, I.d.P.R. Moreira, R. Castillo, J. Llanos, Electronic, structural, and optical properties of host materials for inorganic phosphors, J. Alloys Compd. 513 (2012) 630-640.

[46] J.M. Soler, E. Artacho, J.D. Gale, A. García, J. Junquera, P. Ordejón, D. Sánchez-Portal, The SIESTA method for ab-initio order-N materials simulation, J. Phys.: Condens. Matter. 14 (2002) 2745-2779.

[47] D. Sánchez-Portal, P. Ordejón, E. Canadell, Computing the properties of materials from first principles with SIESTA, Structure and Bonding 113 (2004) 103-170.

[48] For further details on the SIESTA program visit: https://www.icmab.es/siesta

[49] D.M. Ceperley, B.J. Alder, Quantum Monte Carlo calculation of the homogeneous electron gas, Phys. Rev. Lett. 45 (1980) 566-569.

[50] J.P. Perdew, A. Zunger, Self-interaction correction to density-functional approximations for many-electron systems, Phys. Rev. B 23 (1981) 5048-5079.

[51] J.P. Perdew, K. Burke, M. Ernzerhof, Generalized Gradient Approximation Made Simple, Phys. Rev. Lett. 77 (1996) 3865-3868.

[52] J.P. Perdew, A. Ruzsinszky, G.I. Csonka, O.A. Vydrov, G.E. Scuseria, L.A. Constantin, X. Zhou, K. Burke, Restoring the Density-Gradient Expansion for Exchange in Solids and Surfaces, Phys. Rev. Lett. 100 (2008) 136406.

[53] J. Hubbard, Electron Correlations in Narrow Energy Bands, Proc. R. Soc. London, Ser. A 276 (1963) 238-257.

[54] S.L. Dudarev, G.A. Botton, S.Y. Savrasov, C.J. Humphreys, A.P. Sutton, Electron-energy-loss spectra and the structural stability of nickel oxide: An LSDA+U study, Phys. Rev. B 57 (1998) 1505-1509.

[55] N. Troullier, J.L. Martins, Efficient pseudopotentials for plane-wave calculations, Phys. Rev. B 43 (1991) 1993-2006.

[56] L. Kleinman, D.M. Bylander, Efficacious Form for Model Pseudopotentials, Phys. Rev. Lett. 48 (1982) 1425-1428.

[57] E. Artacho, D. Sańchez-Portal, P. Ordejoń, A. García, J.M. Soler, Linear-Scaling ab-initio Calculations for Large and Complex Systems, Phys. Status Solidi B 215 (1999) 809-817.

[58] H.J. Monkhorst, J.D. Pack, Special points for Brillouin-zone integrations, Phys. Rev. B 13 (1976) 5188-5192.

[59] H. Zabrodsky, S. Peleg, D. Avnir, Continuous Symmetry Measures, J. Am. Chem. Soc. 114 (1992) 7843-7851.

[60] M. Pinsky, D. Avnir, Continuous symmetry measures. 5. The classical polyhedra, Inorg. Chem. 37 (1998) 5575-5582.

[61] D. Casanova, J. Cirera, M. Llunell, P. Alemany, D. Avnir, S. Alvarez, Minimal Distortion Pathways in Polyhedral Rearrangements, J. Am. Chem. Soc. 126 (2004) 1755-1763.

[62] M. Pinsky, D. Casanova, P. Alemany, S. Alvarez, D. Avnir, C. Dryzun, Z. Kizner, A. Sterkin, Symmetry operation measures, J. Comp. Chem. 29 (2008) 190-197.

[63] M. Pinsky, C. Dryzun, D. Casanova, P. Alemany, D. Avnir, Analytical Methods for Calculating Continuous Symmetry Measures and the Chirality Measure, J. Comp. Chem. 29 (2008) 2712-2721.

[64] S. Alvarez, D. Avnir, M. Llunell, M. Pinsky, Continuous symmetry maps and shape classification. The case of six-coordinated metal compounds, New J. Chem. 26 (2002) 996-1009.

[65] S. Alvarez, P. Alemany, D. Casanova, J. Cirera, M. Llunell, D. Avnir, Shape maps and polyhedral interconversion paths in transition metal chemistry, Coord. Chem. Rev. 249 (2005) 1693-1708

[66] K.M. Ok, P.S. Halasyamani, D. Casanova, M. Llunell, P. Alemany, S. Alvarez, Distortions in octahedrally coordinated d(0) transition metal oxides: A continuous symmetry measures approach, Chem. Mater. 18 (2006) 3176-3183.

[67] D. Casanova, J.M. Bofill, P. Alemany, S. Alvarez, Shape and symmetry of heptacoordinate transition-metal complexes: Structural trends, Chem. Eur. J. 9 (2003) 1281-1295.

[68] D. Casanova, M. Llunell, P. Alemany, S. Alvarez, The rich stereochemistry of eight-vertex polyhedra: A continuous shape measures study, Chem. Eur. J. 11 (2005) 1479-1494.

[69] H.J. Borchardt, Yttrium-Tungsten Oxides, Inorg. Chem. 2 (1963) 170-173.

[70] J. Huang, J. Xu, H. Li, H. Luo, X. Yu, Y. Li, Determining the structure of tetragonal Y_2WO_6 and the site occupation of Eu^{3+} dopant, J. Sol. State Chem. 184 (2011) 843-847.

[71] V.A. Efremov, A.V. Tyulin, V.K. Trunov, O.V. Kudin, V.K. Yanovskii, V.I. Voronkova, Crystal structure of monoclinic Y_2WO_6 and Yb_2WO_6, Sov. Phys. Crystallogr. (Engl. Transl.) 29 (1984) 534-537.

[72] L.H. Brixner, A.W. Sleight, C.M. Foris, Refined Cell Parameters of the Ln_2WO_6-Type Rare Earth Tungstates, J. Sol. State Chem. 7 (1973) 418-421.

[73] J.-H. Koh, E. Sorge, T.-C. Wen, D.K. Shetty, Thermal expansion behaviors of yttrium tungstates in the WO_3–Y_2O_3 system, Ceram. Int. 39 (2013) 8421-8427.

[74] A.V. Tyulin, V.A. Efremov, V.K. Trunov, Polymorphism of oxytungstates TR_2WO_6 - Mechanisms of structural transformations in Y_2WO_6, Kristallografiya 34 (1989) 885-892.

[75] J.C. Bailar, Some problems in the stereochemistry of coordination compounds: Introductory lecture, J. Inorg. Nucl. Chem. 8 (1965) 165-175.

[76] O. Beaury, M. Faucher, G. Teste de Sagey, P. Caro, Investigation of a New Structural Type for Y_2WO_6, Mat. Res. Bull. 13 (1978) 953-957.

[77] O. Beaury, M. Faucher, G.T. De Sagey, The Structure of Yttrium Tungstate ε-Y_2WO_6, Acta Crystallogr. B 37 (1981) 1166-1170.

[78] N.A. McDowell, K.S. Knight, P. Lightfoot, Unusual High-Temperature Structural Behaviour in Ferroelectric Bi_2WO_6, Chem. Eur. J. 12 (2006) 1493-1499.

[79] R.D. Shannon, Revised Effective Ionic Radii and Systematic Studies of Interatomie Distances in Halides and Chaleogenides, Acta Cryst. A 32 (1976) 751-767.

[80] L.S. Cavalcante, V.M. Longo, J.C. Sczancoski, M.A.P. Almeida, A.A. Batista, J.A. Varela, M.O. Orlandi, E. Longo, M. Siu Li, Electronic structure, growth mechanism and photoluminescence of $CaWO_4$ crystals, CrystEngComm 14 (2012) 853-868.

[81] D.A. Spassky, A.N. Vasil'ev, I.A. Kamenskikh, V.V. Mikhailin, A.E. Savon, Y.A. Hizhnyi, S.G. Nedilko, P.A. Lykov, Electronic structure and luminescence mechanisms in $ZnMoO_4$ crystals, J. Phys.: Condens. Matter 23 (2011) 365501.

[82] B. Ding, C. Han, L. Zheng, C. Zhang, T. J.-P., R. Wang, Z. Tang, Tuning oxygen vacancy photoluminescence in monoclinic Y_2WO_6 by selectively occupying yttrium sites using lanthanum, Sci. Rep. 5 (2015) 9443.

[83] H.M. van Noort, T.J.A. Popma, Concentration-dependent site occupancy dependency in europium-doped Y_2WO_6 as studied by ^{151}Eu Mössbaurer spectroscopy, Sol. State Commun. 55 (1985) 77-79.

Supplementary material for:

Electronic, structural, and optical properties of Y_2WO_6, a host material for inorganic phosphors

Pere Alemany [a] *and Jaime Llanos* [b]

Departament de Ciència dels Materials i Química Física and Institut de Química Teòrica i Computacional (IQTCUB), Universitat de Barcelona, Diagonal 647, 08028 Barcelona, Spain;

Departamento de Química, Universidad Católica del Norte, Avda. Angamos 0610, Casilla 1280, Antofagasta, Chile.

method	a (Å)	b (Å)	c (Å)	β (º)	V (Å^3)
LDA	7.586 (0.0 %)	5.328 (-0.1 %)	11.357 (0.0 %)	104.9 (0.4 %)	443.6 (-0.3 %)
PBE	7.695 (1.4 %)	5.404 (1.3 %)	11.508 (1.4 %)	104.5 (0.1 %)	463.4 (4.1 %)
PBEsol	7.632 (0.6 %)	5.358 (0.5 %)	11.412 (0.5 %)	104.7 (0.3 %)	451.3 (1.4 %)
exp.	7.589	5.334	11.354	104.4	445.1

Table S1 Optimized and experimental [1] structural parameters (relative errors in parentheses) for the monoclinic **m-13** polymorph of Y_2WO_6.

method	a (Å)	b (Å)	c (Å)	V (Å^3)
LDA	5.207 (-0.3 %)	9.015 (-0.2 %)	9.888 (-0.3 %)	464.1 (-0.7 %)
PBE	5.284 (1.2 %)	9.140 (1.2 %)	10.040 (1.3 %)	484.9 (3.7 %)
PBEsol	5.240 (0.4%)	9.058 (0.3 %)	9.943 (0.3 %)	471.9 (1.0 %)
exp.	5.221	9.029	9.915	467.4

Table S2 Optimized and experimental [2] structural parameters for the orthorhombic (Z = 4) **o-19** polymorph of Y_2WO_6. Deviations with respect to the experimental structure are given in parentheses.

method	a (Å)	b (Å)	c (Å)	V ($Å^3$)
LDA	8.499 (-1.1 %)	20.742 (-0.5 %)	5.217 (-0.3 %)	919.7 (-1.8 %)
PBE	8.685 (1.1 %)	21.038 (1.0 %)	5.283 (0.9 %)	965.3 (3.0 %)
PBEsol	8.579 (-0.1%)	20.836 (0.0%)	5.246 (0.2 %)	937.6 (0.1 %)
exp.	8.591	20.840	5.233	936.9

Table S3 Optimized and experimental [3] structural parameters for the orthorhombic **o-19-z8** polymorph of Y_2WO_6.

compound	method	a (Å)	b (Å)	c (Å)	V ($Å^3$)
Bi_2WO_6	PBEsol	5.483 (-0.1%)	5.462 (0.0%)	16.850 (2.2%)	504.7 (2.2%)
	exp.	5.488	5.461	16.484	494.0
Y_2WO_6	LDA	5.462	5.408	15.674	463.0
	PBE	5.593	5.544	15.805	490.1
	PBEsol	5.510	5.463	15.701	472.6

Table S4 Optimized and experimental [4] structural parameters for the orthorhombic (Aurivillius) low temperature phase for Bi_2WO_6 and optimized structural parameters for the **o-29** polymorph of Y_2WO_6.

method	a (Å)	c (Å)	V (Å^3)
LDA	5.299 (0.7 %)	16.233 (-3.6 %)	455.8 (-2.1 %)
PBE	5.388 (2.4 %)	16.419 (-2.5 %)	476.6 (2.4 %)
PBEsol	5.333 (1.4%)	16.305 (-3.2 %)	463.7 (-0.4 %)
exp.	5.260	16.832	465.6

Table S5 Optimized and experimental [5] structural parameters for the tetragonal **t-129** polymorph of Y_2WO_6.

phase	Y site	$d_{M\text{-}O}$ (Å)	coord. n.	Q (Y)	W site	dW-O (Å)	Q(W)
m-13	Y1	2.357	8	+1.27	W1	1.968	+2.26
	Y2	2.375	8	+1.34			
	Y3	2.360	7	+1.37			
o-19-z4	Y1	2.332	7	+1.36	W1	1.951	+2.15
	Y2	2.331	7	+1.46			
o-19-z8	Y1	2.460	8	+1.31	W1	1.956	+2.18
	Y2	2.416	8	+1.37	W2	1.965	+2.23
	Y3	2.286	7	+1.49			
	Y4	2.364	8	+1.29			
o-29	Y1	2.449	8	+1.22	W1	2.054	+2.12
	Y2	2.318	7	+1.26			
t-129	Y1	2.302	6	+1.42	W1	1.965	+2.23
	Y2	2.365	8	+1.25			

Table S6 Net charges obtained from a Mulliken population analysis for the different Y and W sites in the five studied polymorphs of Y_2WO_6.

site		E_{in}(eV)	$d_{M\text{-}O}$ (Å)	S(COC)	S(CTP)	S(CU)	S(SAP)	S(TDD)	S(C_i)
Y1 (2e)	initial	6.34	2.355	-	-	2.674	4.370	2.716	2.140
	relaxed	3.99	2.573			3.733	4.136	2.678	2.530
Y2 (2f)	initial	5.51	2.373	-	-	4.926	1.680	1.806	4.871
	relaxed	3.37	2.588			4.638	2.066	2.194	4.589
Y3 (4g)	initial	6.29	2.305	1.822	1.667	-	-	-	15.992
	relaxed	3.80	2.551	2.789	2.788				15.113

Table S7 Insertion energies and structural parameters for Eu^{3+} in the three different Y^{3+} sites of the PBEsol optimized structure for the monoclinic **m-13** polymorph of Y_2WO_6 before (initial) and after (relaxed) structural relaxation. The $d_{M\text{-}O}$ values indicated in the fourth column refer to average M-O distances for each polyhedron. Labels for reference polyhedra used in the shape analysis are: for coordination number 7, COC for the capped octahedron and CTP for the capped trigonal prism; and for coordination number 8, CU for the cube, SAR for the square antiprism, and TDD for the triangular dodecahedron. The *S(C_i)* value in the last column corresponds to the departure from inversion symmetry as measured by the corresponding CSM.

site		E_{in}(eV)	$d_{M\text{-}O}$ (Å)	S(COC)	S(CPT)	S(C_i)
Y1 (4a)	initial	5.52	2.332	2.273	2.221	16.453
	relaxed	3.12	2.600	3.859	3.662	16.136
Y2 (4a)	initial	6.04	2.331	2.960	1.866	21.209
	relaxed	3.44	2.601	3.013	2.201	21.804

Table S8 Insertion energies and structural parameters for Eu^{3+} in the two different Y^{3+} sites of the PBEsol optimized structure for the orthorhombic **o-19-z4** polymorph of Y_2WO_6 before (initial) and after (relaxed) structural relaxation. The $d_{M\text{-}O}$ values indicated in the fourth column refer to average M-O distances for each polyhedron. Labels for reference polyhedra used in the shape analysis for coordination number 7 are: COC for the capped octahedron and CTP for the capped trigonal prism. The *S*(C_i) value in the last column corresponds to the departure from inversion symmetry as measured by the corresponding CSM.

site		E_{in}(eV)	$d_{M\text{-}O}$ (Å)	S(COC)	S(CTP)	S(CU)	S(SAP)	S(TDD)	$S(C_i)$
Y1 (4a)	initial	2.98	2.460	-	-	4.541	5.916	3.171	4.074
	relaxed	2.93	2.631			4.909	5.515	2.899	4.598
Y2 (4a)	initial	3.18	2.416	-	-	6.403	4.581	2.516	4.559
	relaxed	3.16	2.620			6.803	5.317	3.108	4.447
Y3 (4a)	initial	4.10	2.286	0.783	2.361	-	-		20.087
	relaxed	4.03	2.561	2.473	3.206				17.893
Y2 (4a)	initial	4.11	2.364	-	-	1.598	6.778	3.929	1.412
	relaxed	4.03	2.565			1.978	6.050	3.216	1.654

Table S9 Insertion energies and structural parameters for Eu^{3+} in the four different Y^{3+} sites of the PBEsol optimized structure for the orthorhombic **o-19-z8** polymorph of Y_2WO_6 before (initial) and after (relaxed) structural relaxation. The $d_{M\text{-}O}$ values indicated in the fourth column refer to average M-O distances for each polyhedron. Labels for reference polyhedra used in the shape analysis are: for coordination number 7, COC for the capped octahedron and CTP for the capped trigonal prism; and for coordination number 8, CU for the cube, SAR for the square antiprism, and TDD for the triangular dodecahedron. The $S(C_i)$ value in the last column corresponds to the departure from inversion symmetry as measured by the corresponding CSM.

site		E_{in}(eV)	$d_{M\text{-}O}$ (Å)	S(COC)	S(CTP)	S(CU)	S(SAP)	S(TDD)	$S(C_i)$
Y1	initial	5.88	2.449	-	-	3.168	5.964	4.261	2.261
	relaxed	3.23	2.630			2.222	5.879	3.628	1.849
Y2	initial	6.26	2.318	1.973	2.860	-	-	-	16.486
	relaxed	3.45	2.636	3.014	3.742				15.243

Table S10 Insertion energies and structural parameters for Eu^{3+} in the four different Y^{3+} sites of the PBEsol optimized structure for the orthorhombic **o-29** polymorph of Y_2WO_6 before (initial) and after (relaxed) structural relaxation. The $d_{M\text{-}O}$ values indicated in the fourth column refer to average M-O distances for each polyhedron. Labels for reference polyhedra used in the shape analysis are: for coordination number 7, COC for the capped octahedron and CTP for the capped trigonal prism; and for coordination number 8, CU for the cube, SAR for the square antiprism, and TDD for the triangular dodecahedron. The *$S(C_i)$* value in the last column corresponds to the departure from inversion symmetry as measured by the corresponding CSM.

site		E_{in}(eV)	$d_{M\text{-}O}$ (Å)	S(OC)	S(TP)	S(CU)	S(SAP)	S(TDD)	$S(C_i)$
Y1 (2c)	initial	5.31	2.302	18.033	1.998	-	-	-	16.383
	relaxed	2.72	2.595	20.286	4.935				17.742
Y2 (2a)	initial	5.65	2.390	-	-	0.142	11.032	7.975	0.095
	relaxed	3.69	2.561			0.384	11.120	7.974	0.099

Table S11 Insertion energies and structural parameters for Eu^{3+} in the two different Y^{3+} sites of the PBEsol optimized structure for the tetragonal **t-129** polymorph of Y_2WO_6 before (initial) and after (relaxed) structural relaxation. The $d_{M\text{-}O}$ values indicated in the fourth column refer to average M-O distances for each polyhedron. Labels for reference polyhedra used in the shape analysis are: for coordination number 6, OC for the octahedron and TP for the trigonal prism; and for coordination number 8, CU for the cube, SAR for the square antiprism, and TDD for the triangular dodecahedron. The *$S(C_i)$* value in the last column corresponds to the departure from inversion symmetry as measured by the corresponding CSM.

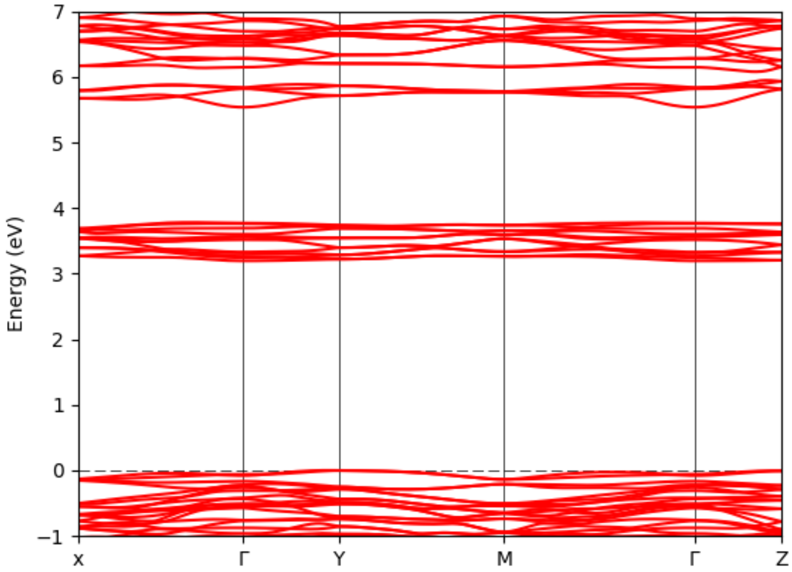

Fig. S1 Band structure calculated for the optimized structure of the **o-19** polymorph of Y_2WO_6 using the PBEsol method.

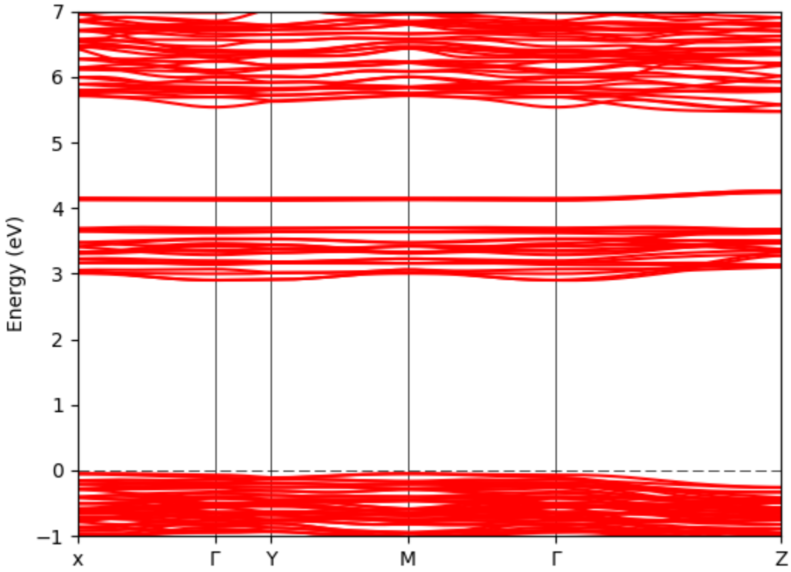

Fig. S2 Band structure calculated for the optimized structure of the **o-19-z8** polymorph of Y_2WO_6 using the PBEsol method.

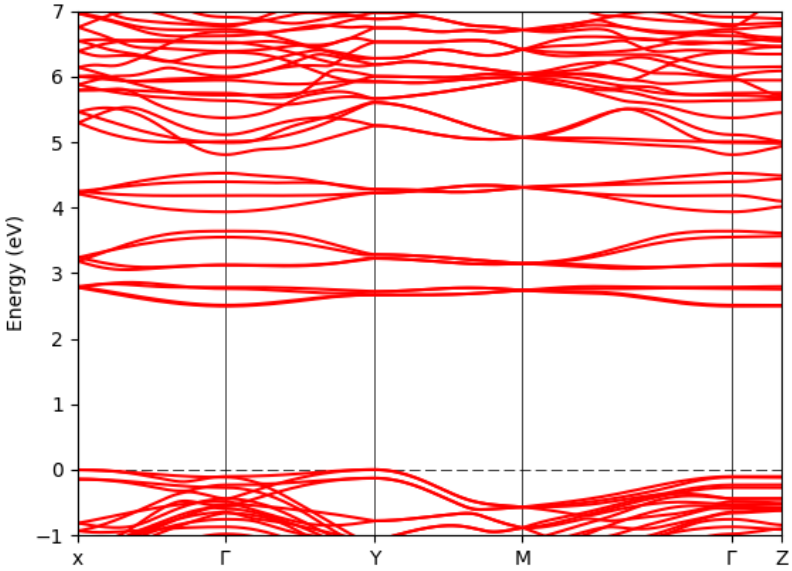

Fig. S3 Band structure calculated for the optimized structure of the **o-29** polymorph of Y_2WO_6 using the PBEsol method.

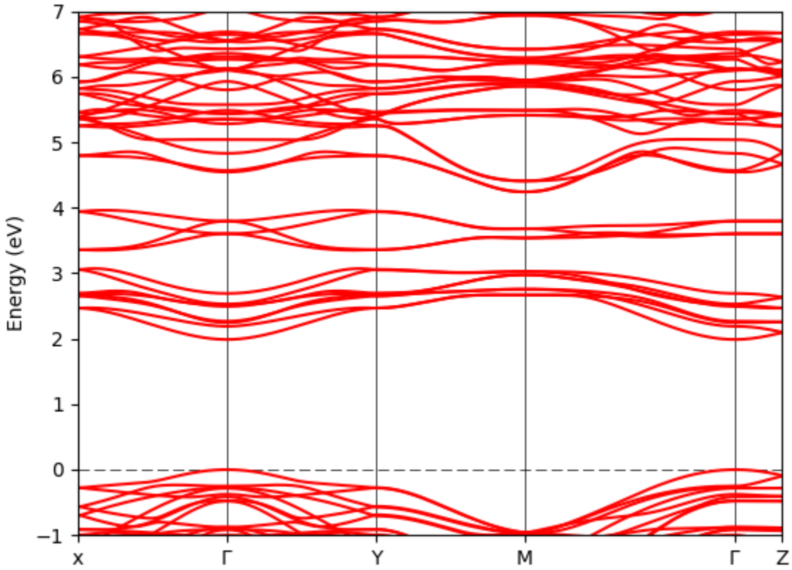

Fig. S4 Band structure calculated for the optimized structure of the **t-129** polymorph of Y_2WO_6 using the PBEsol method.

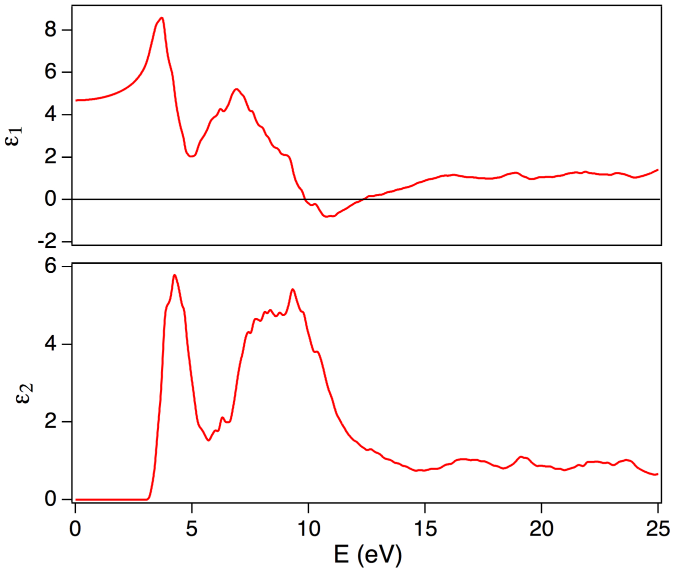

Fig. S5 Real (ε_1) and imaginary (ε_2) parts of the dielectric function calculated for the optimized structure of the **o-19** polymorph of Y_2WO_6, using the PBEsol functional.

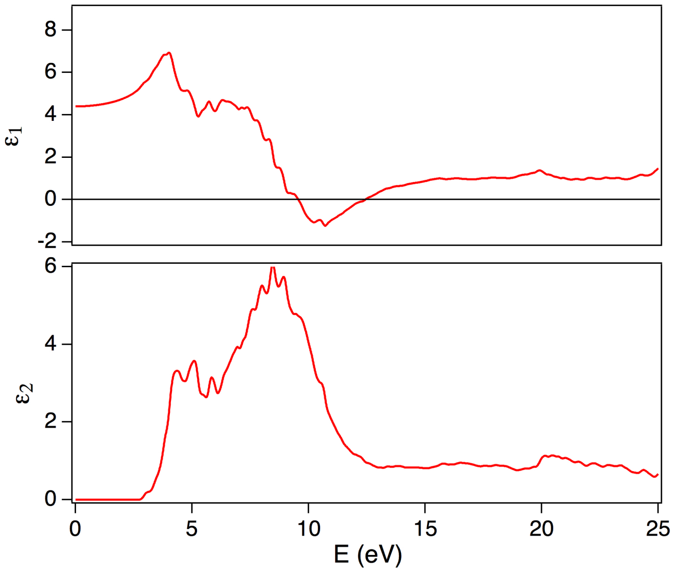

Fig. S6 Real (ε_1) and imaginary (ε_2) parts of the dielectric function calculated for the optimized structure of the **o-29** polymorph of Y_2WO_6, using the PBEsol functional.

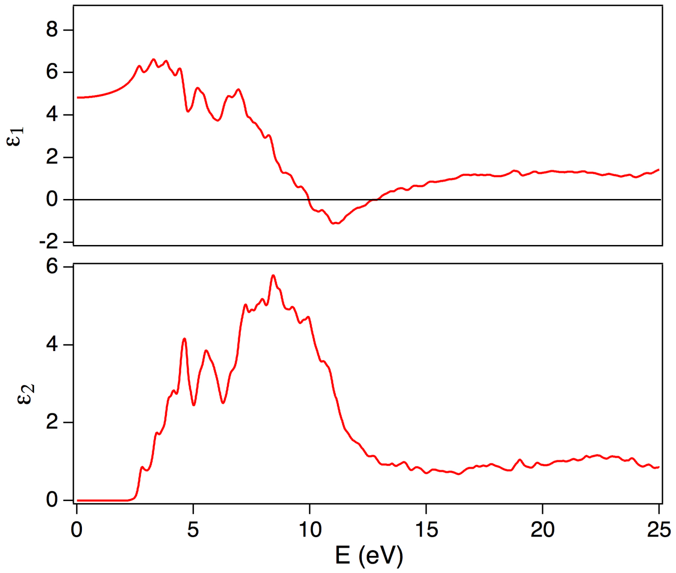

Fig. S7 Real (ε1) and imaginary (ε2) parts of the dielectric function calculated for the optimized structure of the **t-129** polymorph of Y_2WO_6, using the PBEsol functional.

References

[1] V.A. Efremov, A.V. Tyulin, V.K. Trunov, O.V. Kudin, V.K. Yanovskii, V.I. Voronkova, Crystal structure of monoclinic Y_2WO_6 and Yb_2WO_6, Sov. Phys. Crystallogr. (Engl. Transl.) 29 (1984) 534-537.

[2] A.V. Tyulin, V.A. Efremov, V.K. Trunov, Polymorphism of oxytungstates TR_2WO_6 - Mechanisms of structural transformations in Y_2WO_6, Kristallografiya 34 (1989) 885-892.

[3] O. Beaury, M. Faucher, G.T. De Sagey, The Structure of Yttrium Tungstate ε-Y_2WO_6, Acta Crystallogr. B 37 (1981) 1166-1170.

[4] N.A. McDowell, K.S. Knight, P. Lightfoot, Unusual High-Temperature Structural Behaviour in Ferroelectric Bi_2WO_6, Chem. Eur. J. 12 (2006) 1493-1499.

[5] J. Huang, J. Xu, H. Li, H. Luo, X. Yu, Y. Li, Determining the structure of tetragonal Y_2WO_6 and the site occupation of Eu^{3+} dopant, J. Sol. State Chem. 184 (2011) 843-847.